Article

Molecular Cell

# Epigenetic Control of Expression Homeostasis during Replication Is Stabilized by the Replication Checkpoint

## Graphical Abstract

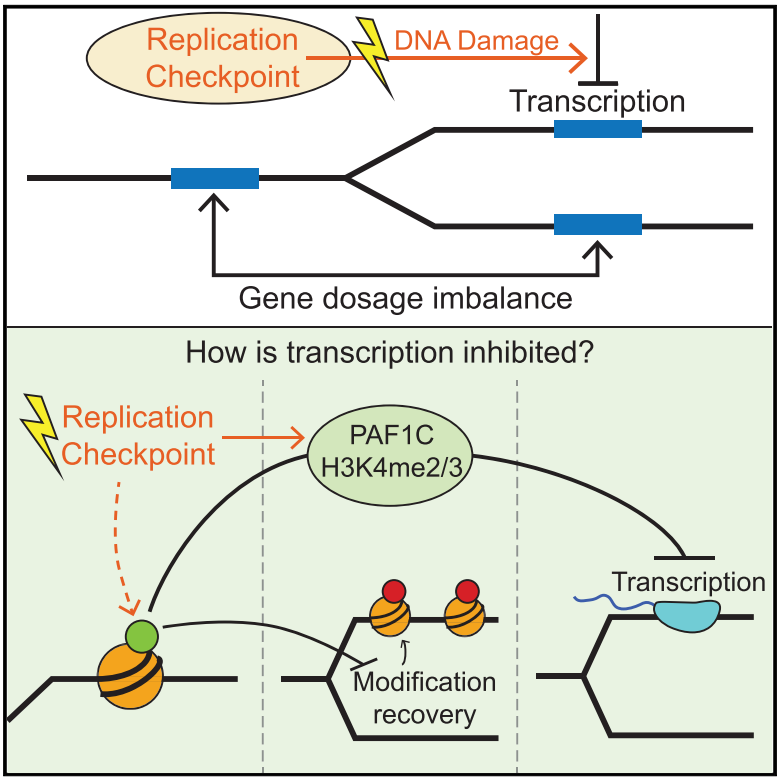


## Authors

Yoav Voichek, Karin Mittelman, Yulia Gordon, Raz Bar-Ziv, David Lifshitz Smit, Rom Shenhav, Naama Barkai

## Correspondence

naama.barkai@weizmann.ac.il

## In Brief

Voichek et al. identified the molecular mechanism inhibiting transcription from replicated genes during DNA replication. The identified circuit utilizes histone modifications and includes the transcription elongation complex PAF1C. The replication checkpoint orchestrates this response in replication-stressed cells. Their work suggests buffering depends on delayed post-replication recovery of histone modifications.

## Highlights

- Yeast arrested with their genome partially replicated maintain expression homeostasis
- Inhibiting replicated gene expression depends on PAF1C and H3K4me downstream of H3K56ac
- Expression homeostasis may result from delayed post-replication recovery of H3K4me
- The replication checkpoint buffers expression via PAF1C and H3K56ac upon DNA damage

Voichek et al., 2018, Molecular Cell *70*, 1–13
June 21, 2018 
https://doi.org/10.1016/j.molcel.2018.05.015

CellPress

Please cite this article in press as: Voichek et al., Epigenetic Control of Expression Homeostasis during Replication Is Stabilized by the Replication Checkpoint, Molecular Cell (2018), https://doi.org/10.1016/j.molcel.2018.05.015

Molecular Cell
Article

CellPress

# Epigenetic Control of Expression Homeostasis during Replication Is Stabilized by the Replication Checkpoint

Yoav Voichek,[1,2] Karin Mittelman,[1,2] Yulia Gordon,[1] Raz Bar-Ziv,[1] David Lifshitz Smit,[1] Rom Shenhav,[1] and Naama Barkai[1,3,*]
[1]Department of Molecular Genetics, Weizmann Institute of Science, Rehovot 76100, Israel
[2]These authors contributed equally
[3]Lead Contact
*Correspondence: naama.barkai@weizmann.ac.il
https://doi.org/10.1016/j.molcel.2018.05.015

## SUMMARY

**DNA replication introduces a dosage imbalance between early and late replicating genes. In budding yeast, buffering gene expression against this imbalance depends on marking replicated DNA by H3K56 acetylation (H3K56ac). Whether additional processes are required for suppressing transcription from H3K56ac-labeled DNA remains unknown. Here, using a database-guided candidate screen, we find that COMPASS, the H3K4 methyltransferase, and its upstream effector, PAF1C, act downstream of H3K56ac to buffer expression. Replicated genes show reduced abundance of the transcription activating mark H3K4me3 and accumulate the transcription inhibitory mark H3K4me2 near transcription start sites. Notably, in hydroxyurea-exposed cells, the S phase checkpoint stabilizes H3K56ac and becomes essential for buffering. We suggest that H3K56ac suppresses transcription of replicated genes by interfering with post-replication recovery of epigenetic marks and assign a new function for the S phase checkpoint in stabilizing this mechanism during persistent dosage imbalance.**

## INTRODUCTION

Cells duplicate their genome during the S phase of the cell cycle, prior to cell division. The process of DNA replication follows a defined temporal order, with some chromosomal domains replicated early in S phase, whereas others are replicated in late S phase. This sequential pattern of replication introduces a transient imbalance in gene dosage, as the copy number of genes that are replicated early increases before that of late-replicating ones. In bacteria, this dosage imbalance propagates to higher expression of early-replicating genes (Beckwith et al., 1966; Schmid and Roth, 1987), a bias that becomes increasingly prominent in rapidly growing cells (Chandler and Pritchard, 1975). One way to exploit this bias is to position genes with DNA damage repair functions close to the origin of replication, thus increasing their expression upon replication-arresting damage, a situation which is indeed observed in various bacteria (Slager et al., 2014). By contrast, eukaryotes buffer the increase in gene dosage so that balanced expression of early- and late-replicating genes is maintained during S phase (Elliott and McLaughlin, 1978; Padovan-Merhar et al., 2015; Voichek et al., 2016). This prevents the possible deleterious consequences of large-scale dosage imbalances observed, for example, upon erroneous duplication of a single chromosome (Torres et al., 2007).

Conditions that challenge genome integrity, such as DNA damage or nucleotide depletion, arrest cells at mid-S phase with their genome partially replicated (Koç et al., 2004; Mirkin and Mirkin, 2007). Under these conditions, the gene dosage imbalance introduced by partial DNA replication persists for an extended period of time. Buffering this dosage imbalance by suppressing transcription from replicated DNA may therefore be particularly important and perhaps more challenging under conditions of replication stress. We recently found that buffering is maintained, and in fact becomes more efficient, under such conditions (Voichek et al., 2016). Thus, whereas unperturbed cycling cells still show a small, yet significant, S phase-specific increase in the expression of early-replicated genes, cells that are arrested at mid-S phase following treatment with the nucleotide-depleting drug hydroxyurea (HU) maintain precisely balanced expression of early- and late-replicated genes.

In budding yeast, suppression of transcription from replicated DNA depends on the acetylation of histone H3 on lysine 56 (H3K56ac) (Voichek et al., 2016), which is carried out by the acetyltransferase Rtt109 and its co-chaperone Asf1 (Driscoll et al., 2007; Han et al., 2007a). H3K56ac is a hallmark of replicated DNA: it is added to newly synthesized histones prior to their incorporation onto the DNA (Han et al., 2007b) and is removed by the histone deacetylases Hst3 and Hst4 at the end of S phase (Celic et al., 2006). The mechanism by which H3K56ac communicates with the transcription machinery, and whether it directly inhibits RNA polymerase II (Pol II) activity or signals to upstream inhibitory processes, remains unknown.

Cells respond to replication stresses by large-scale reprogramming of cellular activities (Bartek et al., 2004; Zhou and Elledge, 2000). In addition to cell-cycle arrest and replication

slow down, changes in gene expression and protein activity are observed (Gasch et al., 2001). This large-scale response is orchestrated by the S phase checkpoint, whose central components are the stress sensor, Mec1 (ATR), and the checkpoint effector kinase, Rad53 (CHK2; Tercero and Diffley, 2001). The checkpoint plays a critical role in maintaining genome integrity, arresting the cell cycle, inducing the necessary transcriptional response, and regulating deoxynucleotide triphosphate (dNTP) pools (Tercero and Diffley, 2001; Zhou and Elledge, 2000). It is unknown whether the checkpoint is required also for suppressing transcription from replicated DNA in mid-S-arrested cells.

In this study, we set out to define the mechanisms that contribute to the buffering of replication-dependent dosage imbalance, focusing on budding yeast. We show that buffering depends on COMPASS, the H3K4 methyltransferase, and its upstream effector, polymerase-associated factor 1 complex (PAF1C) (Krogan et al., 2003; Miller et al., 2001). H3K4 methylation (H3K4me) is tightly linked with gene expression, being both a cause and a consequence of active transcription (Lauberth et al., 2013; Santos-Rosa et al., 2002). In addition, we find that, under conditions of replication stress, buffering becomes fully dependent on the replication checkpoint. Based on these results, we propose that H3K56ac and the checkpoint coordinate buffering by slowing down the post-replication recovery of H3K4me. Our results provide new insight into the mechanism ensuring expression homeostasis during DNA replication and suggest a new role for the replication checkpoint in maintaining buffering during replication stress.

## RESULTS

### Screening for Candidate Genes Required for Limiting Transcription from Replicated DNA

To better understand the mechanism that suppresses transcription from replicated DNA, we searched for genes required for this buffering. We previously identified the role of H3K56 acetylation in maintaining expression homeostasis by analyzing published transcription profiles of 165 chromatin-related mutants (Lenstra et al., 2011). We now extended this analysis to a newer dataset describing the transcription profiles of 1,484 deletion mutants (Figure 1A; Kemmeren et al., 2014). Although these profiles were measured during asynchronous growth, in which only ~25% of cells are in S phase, candidate genes that are needed for buffering the expression of replicated genes could still be identified, as their deletion specifically increases expression of genes replicated early in this sub-population of S phase cells.

We selected 43 candidates for further analysis (Table S1). First, we considered the genes whose deletion increased the expression of early-replicated genes, as described above. Second, we complemented this list by additional genes suspected to play a role in this process based on their function. The selected candidates were classified into three major groups: cell-cycle control and DNA replication (e.g., Mrc1, Ctf8, and Clb6); chromatin assembly and modification (e.g., Cac1, Set1, and Hos4); and mRNA transcription activity (e.g., Rpb9, Med15, and Paf1). The respective deletion mutants were generated and analyzed as described below.

### Expression Homeostasis in HU-Arrested Cells

We decided to examine the role of the identified candidates under conditions of replication stress for two reasons. First, in *S. cerevisiae*, unperturbed S phase lasts ~20 min, a time that is comparable to mRNA half-life (Miller et al., 2011), whereas cells that are subject to replication stress greatly extend their S phase, thereby allowing time for mRNA to accumulate (Mirkin and Mirkin, 2007). Second, focusing specifically on HU-exposed cells may reveal mechanisms that operate to suppress transcription specifically in mid-S-arrested cells, a biological scenario with an increased need for buffering expression from replicated DNA.

We followed cells arrested to G1 with yeast mating factor (α-factor) and released into 200 mM HU, profiling DNA and mRNA (Figure 1B). Wild-type (WT) and *RTT109*-deleted cells were profiled at a time resolution of 6–10 min, showing the expected cascade of gene expression (Figure 1D). Replicated regions were defined based on DNA sequencing, showing rapid initiation of replication followed by subsequent slower progression (Figure 1C).

We next compared gene expression with the increase in DNA content. In *rtt109Δ* cells, expression of replicated genes increased practically immediately upon the onset of replication, consistent with the loss of expression homeostasis in these cells (Figure 1E). In contrast, long-term arrested WT cells maintained balanced expression of replicated and non-replicated genes, consistent with precise buffering. Of note, during the early phase of replication, WT cells over-compensated for the increase in gene dosage such that expression of replicated genes was lower than that of non-replicated ones (Figure 1E).

### Temporal Dynamics of Transcription and DNA Replication in Screen Candidates during HU Treatment

We next examined the transcription and DNA profiles of our candidate mutants at 30, 90, and 180 min following the release from G1 arrest into HU. In most mutants, transcription dynamics remained similar to WT cells (Figure S1), whereas mutants defective in mRNA synthesis showed a delayed response (e.g., *paf1Δ* and *rpb9Δ*). Replication was perturbed in many mutants (Figure 2A, left panel), as quantified by the estimated average fork velocity and the rates by which replication origins initiated (Figure 2A, mid and right panels). For example, cells deleted of *MRC1* or *CTF8* decreased fork velocity but increased the number of firing origins (Hanna et al., 2001; Osborn and Elledge, 2003). By contrast, perturbing mRNA synthesis by deleting *RPB9* or *PAF1* delayed the onset of replication, reminiscent of the transcription slowdown in these mutants (Figure S1).

As expected, expression homeostasis was lost in all strains defective in H3K56ac (*rtt109Δ*, *asf1Δ*, *rtt109Δtos4Δ*, H3K56A, H3K56Q, and H3K56R; Figure 2B). Four of the candidates involved in replication or cell cycle progression also lost homeostasis: *clb5Δ*, *swi6Δ*, *mrc1Δ*, and *ctf8Δ*. Of the candidates associated with chromatin maintenance, a significant loss of homeostasis was found in mutants deleted of *SET1*, *SWD3*, and *HOS4*. Set1 and Swd3 are two components of the COMPASS histone methyltransferase complex (Miller et al.,

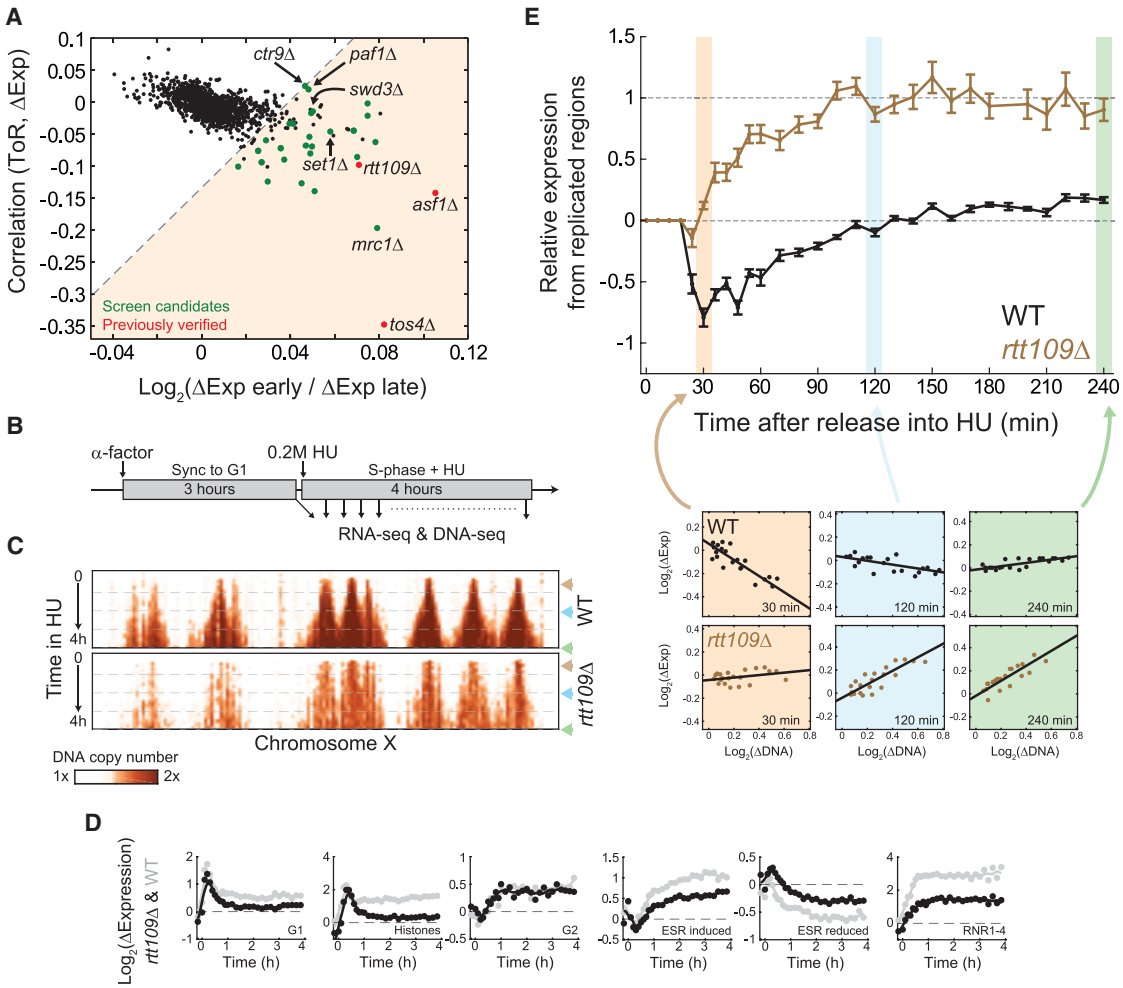


**Figure 1. Screen for Genes Required for Expression Homeostasis**

(A) *In silico* screen for candidates that play a role in expression homeostasis. Correlation between the time of replication (ToR) per gene (Yabuki et al., 2002) and the change in gene expression observed in different yeast deletion mutants (Kemmeren et al., 2014) is plotted against the average difference between the expression of early- and late-replicating genes in the same mutant. Red dots represent strains previously verified for loss of expression homeostasis (Voichek et al., 2016). Green dots in the shaded area represent mutants chosen for further analysis. For list of all strains, see Table S1.

(B) Quantifying expression homeostasis during HU treatment—experimental scheme: see text for details.

(C) Replication progression is similar in WT and *rtt109Δ* strains during HU treatment. Shown is the temporal change in DNA sequence coverage along chromosome 10, normalized to DNA content in G1-synchronized cells (see STAR Methods). X axis represents chromosomal coordinates, and y axis represents time after release from G1 into HU. Brown, blue and green triangles highlight the 30-min and 2- and 4-hr time points of HU treatment, respectively, corresponding to data in (E).

(D) Transcription profiles of WT and *rtt109Δ* strains during HU treatment. Shown are the temporal average changes in expression of genes expressed during G1 or G2 of the cell cycle (Ihmels et al., 2002), histone genes, environmental stress response genes (ESRs) (Gasch et al., 2000), and the RNR1-4 genes, which are responsive to DNA stress (Mulder et al., 2005). Gene expression levels were log2 transformed and normalized by gene expression of cells synchronized to G1 by α-factor.

(E) Expression of replicated genes is buffered in WT cells, but not in *rtt109Δ* cells. The relative expression from replicated regions compared to non-replicated ones was plotted for WT and *rtt109Δ* cells, for every time point during 4 hr of HU treatment. Relative expression from replicated genes was quantified for each time point by comparing the relative changes in gene expression to the respective changes in DNA content. As can be seen in the bottom panel for the 30-min (brown) and 2- (blue) and 4-hr (green) time points, changes in gene expression are linear with changes in DNA content (STAR Methods). Note that, in the absence of buffering, the relation between differences in gene expression and changes in DNA content gives a slope of 1, whereas in the case of full buffering, gene expression does not change, leading to a slope of zero. More generally, expression homeostasis was measured by calculating the value of this slope for each time point. Error bars represent SD over clustering of the DNA to groups of similar replication time using different parameters (STAR Methods).

2001), whereas Hos4 is a component of the SET3 histone deacetylase complex, which is recruited by COMPASS-dependent methylation (Kim and Buratowski, 2009). Finally, of the candidates associated with mRNA transcription, expression homeostasis was lost upon deletion of *PAF1* or *CTR9*, two components of PAF1C (Krogan et al., 2002).

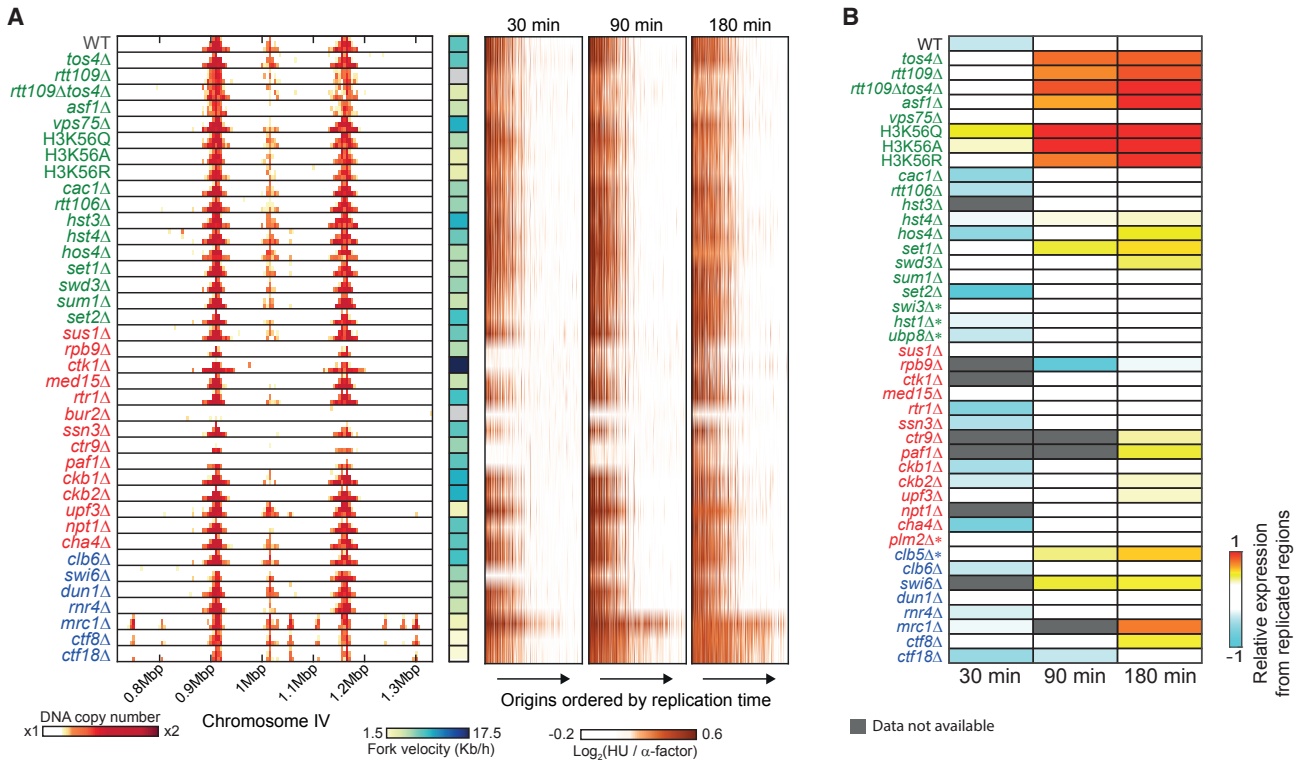


**Figure 2. Screening for Mutants that Lose Expression Homeostasis following HU Treatment**

(A) Replication in mutant strains following HU treatment. Shown is the temporal change in DNA sequence coverage along a segment of chromosome 4 following 30, 90, and 180 min of HU treatment (left). Replication fork velocities were estimated by the spatial progression of replication between the 90 and 180 min time points (middle; see STAR Methods). To compare origin of replication firing between mutants, the ~400 confirmed origins from OriDB (Nieduszynski et al., 2007) were ordered according to their replication time (Yabuki et al., 2002) and their average DNA coverage at the indicated times was plotted (right; see STAR Methods). Strain labels indicate a role in chromatin maintenance (green), a role in mRNA transcription activity (red), and a role in cell cycle control or DNA replication (blue).

(B) Expression homeostasis of candidate genes. The extent of expression homeostasis during HU treatment in each of the strains at each time point was quantified as in Figure 1E and is shown in matrix format. Gray indicates data not available. *bur2Δ* was omitted, as it did not replicate its DNA; no DNA data were available for asterisk-marked strains, and thus, WT DNA was used to calculate buffering levels.

## PAF1C and COMPASS Control Expression Homeostasis Downstream of H3K56ac

PAF1C is a transcription elongation complex that directly associates with Pol II (Krogan et al., 2002) and could therefore be a direct effector that transduces the H3K56ac signal to reduce transcription. Furthermore, PAF1C is essential for the H3K4 methylation activity of COMPASS (Krogan et al., 2003), the second complex identified in our screen. Notably, H3K4me is not only deposited during transcription but also functions as a regulator of gene expression (Lauberth et al., 2013; Santos-Rosa et al., 2002; Soares et al., 2017), with H3K4 tri-methylation (H3K4me3) promoting gene expression, whereas its di-methylation (H3K4me2) plays an inhibitory role (Kim and Buratowski, 2009). PAF1C and COMPASS could therefore function through the same pathway to repress expression from replicated DNA by modulating the H3K4me pattern.

Deletion of *PAF1* has been shown to abolish H3K4 methylation (Krogan et al., 2003). To examine whether it is also required for stabilizing H3K56ac, potentially explaining the loss of homeostasis upon its deletion, we profiled the genome-wide pattern of H3K56ac in WT cells and in cells deleted of *SET1*, *PAF1*, or *CTR9* following HU treatment (Figure 3A). As expected, WT cells accumulated H3K56ac specifically in replicated regions. This precise pattern was also observed in all three mutants, confirming that PAF1C and COMPASS are not required for stabilizing H3K56ac but rather function downstream to this mark.

## H3K4 Tri-methylation on Replicated Genes Is Suppressed in WT, but Not in RTT109-Deleted Cells

If COMPASS or PAF1C contribute to expression homeostasis through their role in H3K4 methylation, then the H3K4me pattern on replicated genes should differ from that found on non-replicated ones. To examine this, we temporally profiled the patterns of H3K4me2 and H3K4me3 in WT cells following HU exposure. Indeed, we observed two notable differences in the pattern of H3K4me on replicated genes. First, H3K4me3 did not increase with gene dosage, similar to the buffering observed for gene expression (Figures 3B and S2A). Second, the spatial pattern of H3K4me2, which is known to inhibit expression, shifted toward the transcription start site of replicated genes (Figures 3C and 3D). This differential pattern of H3K4me on replicated and

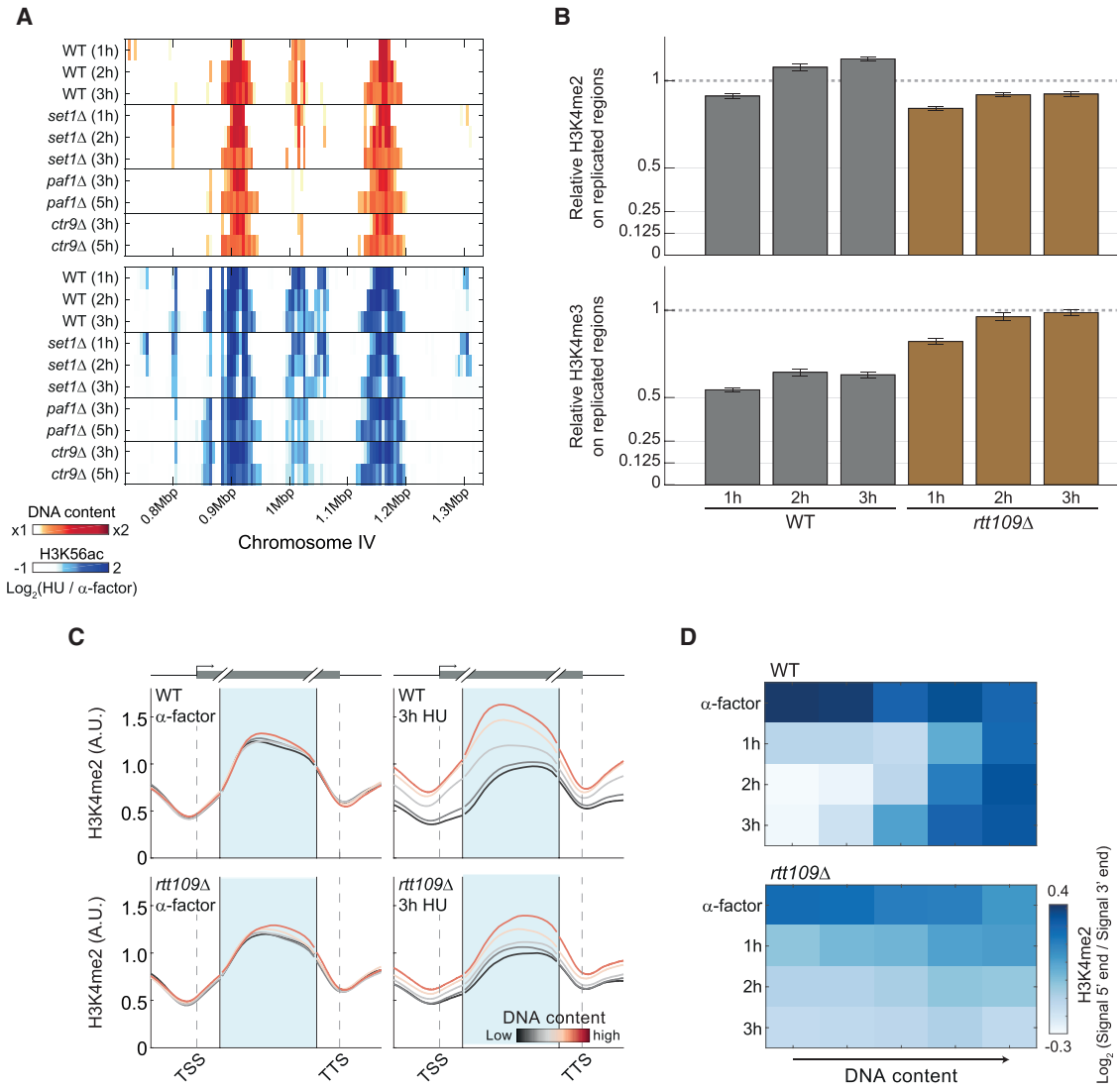


**Figure 3. Replicated Genes Show Differential H3K56ac and H3K4 Methylation Patterns**

(A) H3K56 acetylation is not affected by deletion of SET1, PAF1, or CTR9. The genome-wide pattern of H3K56ac was measured using chromatin immunoprecipitation sequencing (ChIP-seq) at the indicated time points following HU exposure for WT, *set1Δ*, *paf1Δ*, and *ctr9Δ* strains. DNA content (top) and H3K56ac patterns (bottom) are shown on the same segment of chromosome 4, as in Figure 2A, relative to the signal in G1-arrested cells (see also Figure S3H for H3K56ac quantification relative to DNA content).

(B–D) H3K4 methylation on replicated genes differs between WT and *rtt109Δ* cells. The patterns of H3K4me2 and H3K4me3 were profiled for WT and *rtt109Δ* cells following HU treatment.

(B) Methylation levels were normalized by their G1-arrested values. The increase in methylation levels on replicated genes was quantified relative to DNA content as in Figure 1E (STAR Methods). Error bars represent SD.

(C) The metagene pattern of H3K4me2 over gene bodies is shown for gene groups of similar replication timing in WT and *rtt109Δ* (see also Figures S2C and S2D).

(D) The difference between the H3K4me2 signal near the transcription start site (TSS) and near the transcription termination site (TTS), averaged over groups of genes of similar ToR, is shown for the indicated strains and time points following HU exposure (STAR Methods; see also Figures S2E–S2G for H3K4me3 quantification).

non-replicated genes is therefore consistent with H3K4 methylation mediating expression homeostasis.

We next asked whether this pattern of H3K4 methylation on replicated genes depends on H3K56 acetylation. To this end, we measured the pattern of H3K4me2 and 3 in *rtt109Δ* cells. In this mutant, H3K4me3 showed rapid recovery on replicated genes (Figure 3B), and the spatial pattern of H3K4me2 on replicated genes was the same as that of non-replicated ones (Figures 3C and 3D), suggesting that COMPASS functions in expression homeostasis downstream to H3K56ac. Finally, the extent to which expression homeostasis was lost in a mutant deleted of both *RTT109* and *SET1* was the same as in *rtt109Δ* cells

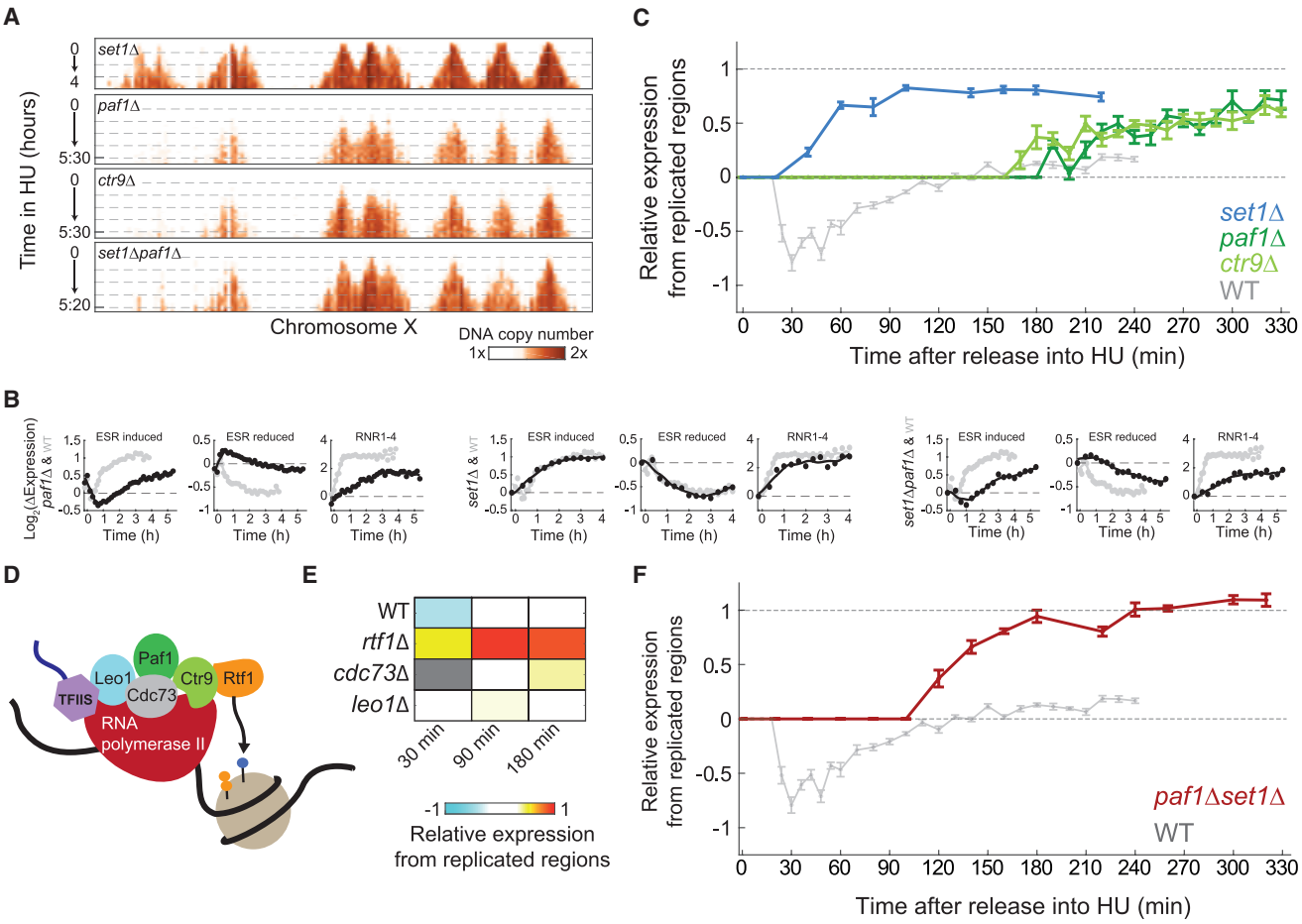


**Figure 4. PAF1C and COMPASS Contribute to Expression Homeostasis through the Same Pathway**

(A) Deletion of *PAF1* or *CTR9* slows the onset of replication. Shown are replication profiles, plotted as in Figure 1C. *paf1Δ*, *ctr9Δ*, and *paf1Δset1Δ* were followed for 5:20 or 5:30 hr to account for their slow replication.

(B) Deletion of *PAF1* or *CTR9* slows the transcriptional response. Expression of the indicated gene groups is shown for the indicated strains as in Figure 1D (see also Figure S3A).

(C) Deletion of PAF1C and COMPASS subunits perturbs expression homeostasis. Relative expression from replicated regions for each strain at each time point was measured as in Figure 1E (see also Figure S2H).

(D and E) Expression homeostasis is lost upon *RTF1* deletion.

(D) Three additional subunits of the PAF1C complex (Xu et al., 2017) not included in our original screen were assayed for expression homeostasis.

(E) Expression homeostasis measurements for *rtf1Δ*, *cdc73Δ*, and *leo1Δ* are plotted in matrix format, as in Figure 2B (see also Figures S3B and S3D–S3F). WT is shown for comparison.

(F) Deletion of both *PAF1* and *SET1* fully abolishes expression homeostasis. Relative expression from replicated regions for *paf1Δset1Δ* is shown as in Figure 1E (see also Figure S3G).

(Figure S3I), confirming that the two processes contribute to expression homeostasis through the same pathway.

## The PAF1C Contribution to Expression Homeostasis Is Partially Explained by Its COMPASS Regulation

To more precisely quantify the contribution of COMPASS and PAF1C to expression homeostasis, we profiled cells deleted of PAF1C and COMPASS subunits at high temporal resolution and for a longer period. *paf1Δ* and *ctr9Δ* were delayed in initiating replication (Figure 4A) or transcription (Figures 4B and S3A). Further, some origins which fired relatively early in the WT background were repressed by *PAF1* or *CTR9* deletion (compare Figures 1C and 4A). By contrast, deletion of *SET1* had a relatively minor effect on replication.

Consistent with our screen results, deletion of either *PAF1* or *CTR9* led to a partial loss of homeostasis, with the expression of replicated genes increasing by ~1.5 ($\approx 2^{0.6}$) fold compared to the two-fold increase seen in *rtt109Δ* cells (Figure 4C). Similarly, deletion of *SET1* led to a higher but still partial effect, increasing expression of replicated genes by ~1.75 fold ($\approx 2^{0.8}$; Figure 4C). Therefore, both PAF1C and COMPASS contribute to expression homeostasis, but each of their contributions is partial. Perturbing the INO80 complex, which was shown to act in parallel to PAF1C in HU-treated cells

(Poli et al., 2016), had no effect on expression homeostasis (Figures S3B and S3C).

PAF1C contains five subunits (Xu et al., 2017; Figure 4D), among which only Paf1 and Ctr9 were included in our screen. If this complex contributes to expression homeostasis by regulating COMPASS activity, then only its subunits found to be essential for H3K4me (Krogan et al., 2003) should show a buffering phenotype. Leo1 and Cdc73 are two additional components of PAF1C that interact with transcription elongation factor TFIIS and Pol II and are not essential for H3K4 methylation (Dermody and Buratowski, 2010; Laribee et al., 2005; Xu et al., 2017). The last subunit, Rtf1, is directly involved in chromatin modification and histone methylation in particular (Dover et al., 2002; Mayekar et al., 2013; Simic et al., 2003). Extending our analysis to these additional subunits, we found that neither Leo1 nor Cdc73 had an effect on expression homeostasis (Figure 4E). By contrast, deletion of *RTF1* had a strong phenotype, indistinguishable from that observed in *rtt109Δ* cells (Figures 4E and S3F).

The complete loss of buffering observed in *rtf1Δ* cells contrasted the partial loss found in *paf1Δ* or *ctr9Δ* cells. This could reflect the faster replication and transcription dynamics of *rtf1Δ* cells (Figures S3D and S3E). More surprising, perhaps, was the partial loss of homeostasis observed in *set1Δ* cells, which suggested that, in addition to directly regulating H3K4me, PAF1C contributes to homeostasis through an additional, Rtf1-dependent mechanism. To this end, we also assayed cells deleted of both *PAF1* and *SET1*. Deletion of *SET1* on the background of *paf1Δ* partially rescued the delay in replication onset (Figure 4A). Notably, this mutant fully lost expression homeostasis, increasing the expression of replicated genes to the same extent as *rtt109Δ* cells (Figure 4F). Together, our results suggest that PAF1C contributes to expression homeostasis primarily by regulating COMPASS-dependent H3K4me but possibly through an additional, Rtf1-dependent process that is independent of this methylation.

## PAF1C and COMPASS Deplete Pol II from Replicated Genes

PAF1C and COMPASS could suppress expression of replicated genes by reducing Pol II binding to replicated genes. To examine this, we profiled the genome-wide binding of Pol II to DNA following HU treatment. In *rtt109Δ* cells, Pol II binding to replicated DNA increased proportionally to gene copy number (Figure 5A). By contrast, WT cells showed only a moderate increase in Pol II binding. Therefore, expression homeostasis is explained, at least in part, by reduced Pol II binding to replicated DNA.

In cells deleted of *PAF1*, *CTR9*, or *SET1*, Pol II binding to replicated DNA increased, but this increase was lower than that observed in *rtt109Δ* cells, whereas in *paf1Δset1Δ* cells, Pol II binding became proportional to gene dosage (Figure 5A). When compared across all mutants, the increase in Pol II binding to replicated genes was correlated with the increase in expression from these regions (Figure 5B). Together, PAF1C and COMPASS contribute to expression homeostasis by reducing Pol II binding to replicated DNA, inhibiting its DNA binding, or promoting its dissociation.

## Expression Homeostasis during Replication Stress Depends on the DNA Replication Checkpoint

As described above, PAF1C contributes to expression homeostasis primarily by regulating COMPASS-dependent H3K4me, with an additional residual contribution that appears COMPASS independent. Recently, it was shown that, specifically in HU-arrested cells, PAF1C triggers Pol II eviction and degradation (Poli et al., 2016). We reasoned that this eviction, if it occurs primarily on replicated DNA, could account for the COMPASS-independent contribution of PAF1C to expression homeostasis, explaining the more efficient buffering observed upon HU treatment compared to unperturbed S phase.

The S phase checkpoint orchestrates the response to replication stress (Zegerman and Diffley, 2009). PAF1C-dependent eviction of Pol II similarly depends on its phosphorylation by the checkpoint sensor Mec1 (ATR; Poli et al., 2016). We therefore examined whether the checkpoint contributes to expression homeostasis, following cells deleted of either *MEC1* or *RAD53* (CHK2), the checkpoint effector kinase. To maintain viability, these mutations were combined with the deletion of RNR inhibitor *SML1* (Chabes et al., 1999), which by itself had no buffering phenotype (Figure S5G). Upon exposure to HU, both checkpoint mutants initiated replication in a normal manner but then arrested rapidly, with less replicated DNA compared to WT cells (Figure 6B).

In unperturbed cycling cells, deletions of either *MEC1* or *RAD53* had no effect on expression homeostasis (Figure 6A). By contrast, following HU treatment, expression homeostasis was fully lost (Figure 6C). Loss of buffering was observed also in *mec1-100* and *mec1-101* mutants, which are defective specifically in the intra-S phase checkpoint activity of Mec1 (Paciotti et al., 2001; Figures S5E–S5G). Deletion of *RAD53* also increased expression of replicated genes to the same extent, but this was observed only after a delay of ~90 min. Further, in both checkpoint mutants, Pol II binding on replicated genes increased in proportion to gene dosage, largely resembling the pattern observed in *rtt109Δ* and *paf1Δset1Δ* cells (Figures 6D and S5D). Mrc1, which also lost buffering in our screen (Figure 2B), has been reported as required for Mec1 accumulation at stalled replication forks (Naylor et al., 2009). Analysis of Mrc1 mutants defective in this function showed full expression homeostasis, indicating that its role in buffering is unrelated to this checkpoint function (Figures S5G and S5H).

## The S Phase Checkpoint Stabilizes H3K56 Acetylation

Expression homeostasis in HU-exposed cells is fully dependent on the replication checkpoint, suggesting that it acts not only through PAF1C but also through an additional pathway. Examining the H3K56ac pattern in checkpoint-deficient cells, we observed that H3K56ac initially accumulated on replicated regions but was then diluted (Figure 6E). Consequently, in later time points, the H3K56ac levels on replicated regions were significantly reduced compared to WT, *paf1Δ*, or *set1Δ* cells. This suggests that the loss of expression homeostasis in the checkpoint mutants depends not only on its regulation of PAF1C but also on stabilization of H3K56ac.

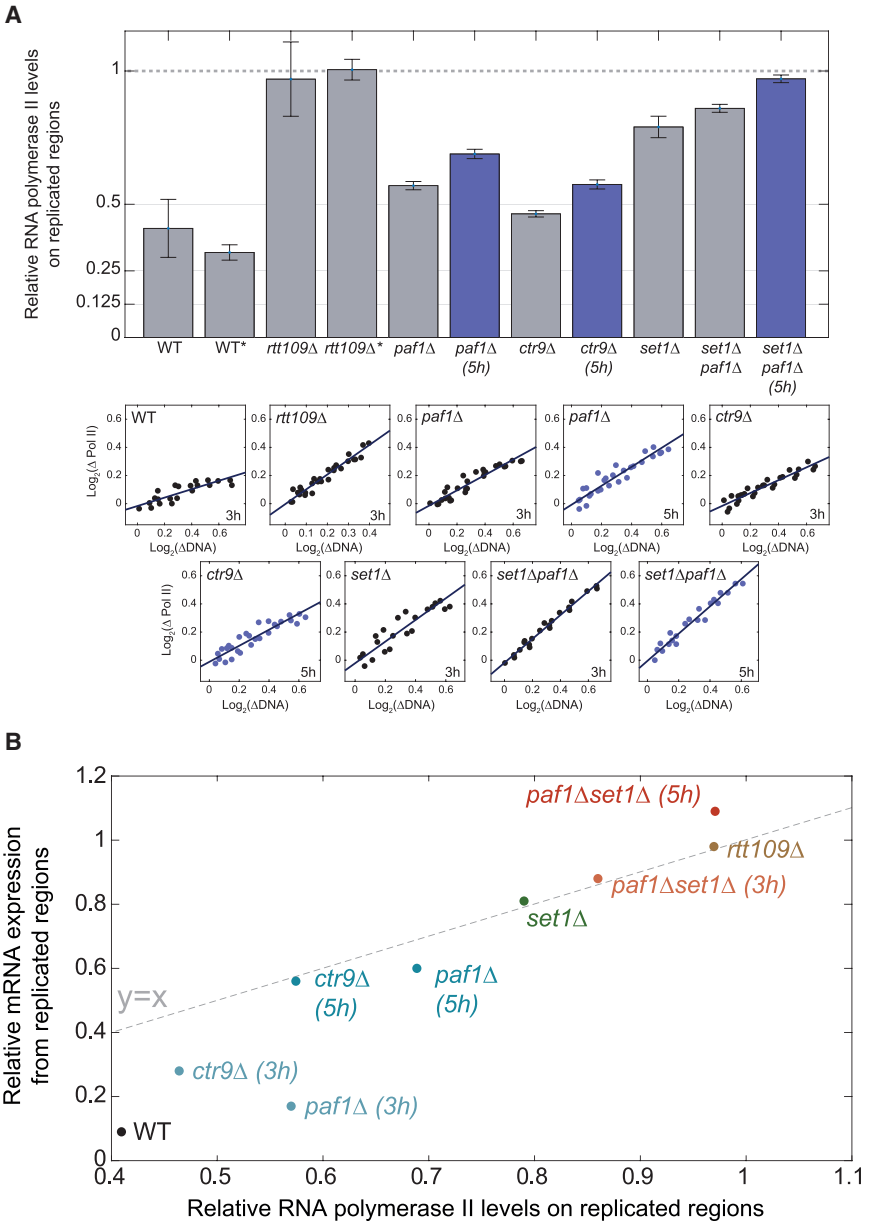


**Figure 5. Depletion of RNA Polymerase II from Replicated Genes Correlates with Expression Homeostasis**

Binding profiles of RNA polymerase II were measured in cells synchronized to G1 and following 3 hr (gray) or 5 hr (blue) after release to HU.

(A) Shown is the extent to which Pol II binds replicated DNA, quantified as in Figure 1E (top). Asterisk-marked WT and *rtt109Δ* cells were profiled after 3 hr of HU treatment with no prior synchronization. (Bottom) Examples of linear fits between the change in Pol II binding and DNA content are shown (see also Figure S4). Error bars represent SD.

(B) Comparison between relative expression and relative Pol II levels from replicated regions of indicated strains.

As shown above, the deposition of the H3K56ac mark onto replicated DNA delays the recovery of the normal H3K4me pattern. We therefore asked whether the checkpoint-deficient mutants show faster recovery of the H3K4me pattern. To this end, we profiled H3K4me2 and H3K4me3 in cells deleted of either *MEC1* or *RAD53* following HU exposure. Recovery of the transcription-activating mark H3K4me3 was faster than that observed in WT cells (Figure 6F). Similarly, the accumulation of the transcription-inhibitory mark H3K4me2 close to the transcription start site (TSS) was not as prominent as that observed in WT cells but was significant when compared to *rtt109Δ* cells (Figure 6G). These partial effects of the checkpoint mutants on the post-replication recovery of H3K4me are therefore consistent with its partial effects on H3K56ac stability.

It was previously reported that Mec1 targets the H3K56ac deacetylase Hst3 to degradation (Edenberg et al., 2014). We reasoned that this degradation could explain the reduced H3K56ac and loss of homeostasis. To this end, we considered *Hst3Δ97*, an Hst3 allele that is resistant to the Mec1-dependent phosphorylation that leads to its degradation (Edenberg et al., 2014). This allele, however, had no effect on expression homeostasis (Figures S5K–S5M).

## DISCUSSION

Gene duplications or genomic manipulations that increase gene dosage lead to higher mRNA production, with deleterious consequences when occurring at large scale (Torres et al., 2007). An exception is the transient increase in gene dosage during DNA replication, which is buffered to maintain balanced gene expression. In this study, we examined the mechanism by which replicated DNA is recognized and how its transcription is suppressed.

Replicated DNA is wrapped around newly synthesized histones that show a unique modification pattern (Benson et al., 2006; Sobel et al., 1995). Certain modifications, such as H3K56ac, are added to histones prior to their incorporation onto the DNA (Driscoll et al., 2007; Han et al., 2007a), whereas others, such as H3K4me3, are not present on newly synthesized histones and, as a consequence, become diluted in replicated regions (Radman-Livaja et al., 2010). The histone modification pattern therefore distinguishes replicated genes and, if stably maintained, could be used to buffer expression.

Previously, we identified a critical role for H3K56ac, a hallmark of replicated DNA, in buffering replicated gene expression (Voichek et al., 2016). Our present study points to a modification acting downstream of H3K56ac, H3K4 methylation, which has

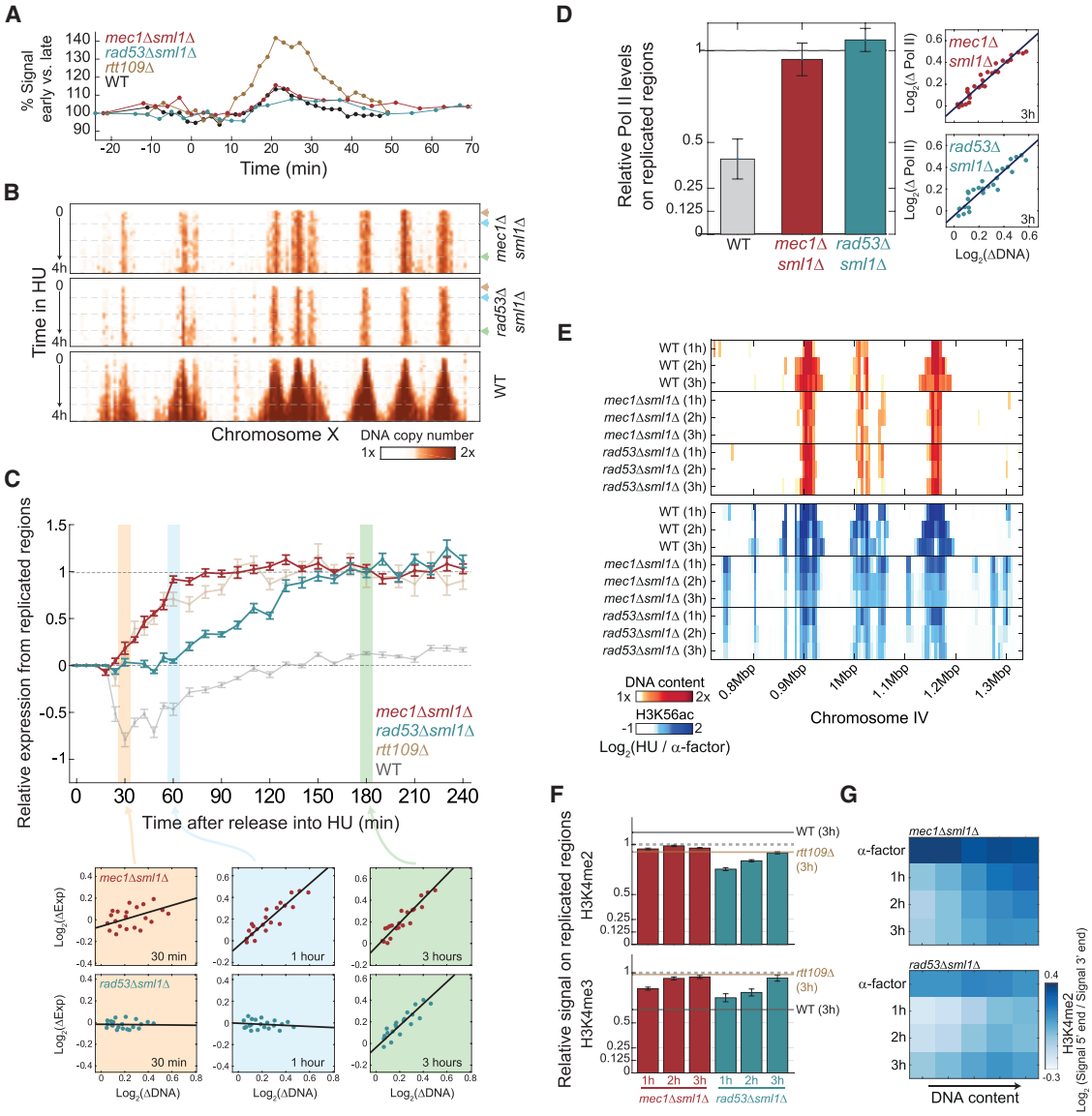


**Figure 6. The DNA Replication Checkpoint Is Required for Expression Homeostasis during HU Treatment**

(A) Expression homeostasis during normal cell cycle does not require Mec1 or Rad53. Average increase in expression of 500 earliest-replicating genes relative to 500 latest-replicating ones is shown for *mec1Δsml1Δ* and *rad53Δsml1Δ* strains, calculated as in Voichek et al. (2016). Cells were synchronized using α-factor and released into rich medium (yeast extract peptone dextrose [YPD]). Time courses were aligned so that t = 0 indicates the beginning of replication. Data for WT and *rtt109Δ* are taken from Voichek et al. (2016) and shown for comparison.

(B) *mec1Δsml1Δ* and *rad53Δsml1Δ* cells arrest replication rapidly upon HU treatment. Shown are the replication profiles, plotted as in Figure 1C. WT data from Figure 1C are shown for comparison. Brown, blue, and green triangles, respectively, highlight the 30-min and 1- and 3-hr time points of HU treatment, corresponding to data in (C) (see Figure S5A for transcription characterization).

(C) Expression homeostasis is lost upon HU treatment of *mec1Δsml1Δ* and *rad53Δsml1Δ*. Relative expression from replicated regions was measured as described in Figure 1E. WT and *rtt109Δ*, shown in Figure 1E, are plotted for comparison (see also Figure S5N for *rtt109Δmec1Δsml1Δ* and *rtt109Δrad53Δsml1Δ*).

(D) Pol II binding on replicated regions in *mec1Δsml1Δ* and *rad53Δsml1Δ* cells increases upon HU treatment: as in Figure 5A, for the indicated strains. WT data from Figure 5A are shown for comparison.

(E) H3K56 acetylation of replicated regions is decreased in *mec1Δsml1Δ* and *rad53Δsml1Δ* cells: as in Figure 3A for the indicated strains. WT data from Figure 3A are shown for comparison (see also Figures S5I and S5J for H3K56ac quantification).

(F and G) H3K4 methylation on replicated genes differs between WT, *mec1Δsml1Δ*, and *rad53Δsml1Δ* cells: as in Figures 3B and 3D for the indicated strains and time points (in F, 3 hr WT and *rtt109Δ* from Figure 3B are shown for comparison; see also Figure S5B for metagene analysis and Figure S5C for H3K4me3 quantification as in G).

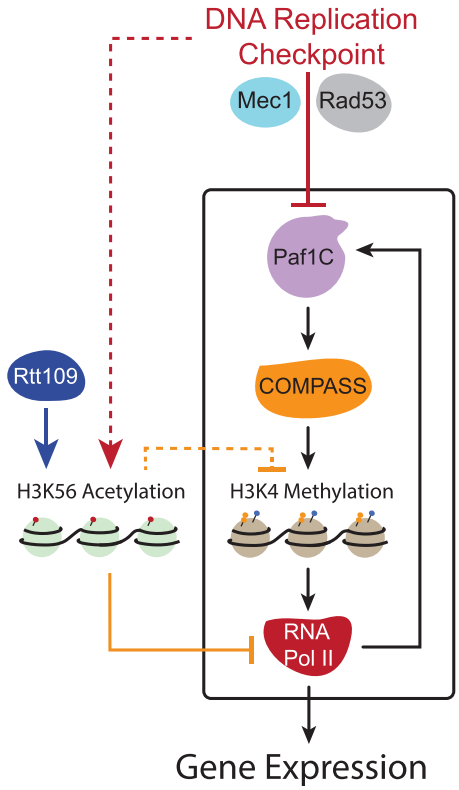


**Figure 7. Model—the Replication Checkpoint Interferes with Post-replication Recovery of Histone Modifications**

Suggested model: PAF1C promotes COMPASS H3K4 methylation activity. H3K4 methylation exerts a positive feedback loop on transcription, replacing the inhibitory H3K4me2 marks with activating H3K4me3 marks. During replication, newly synthesized histones, marked with acetylated H3K56, are incorporated onto the replicated DNA. These new histones are not methylated, and in order to regain maximal transcription following replication, the methylation signal must be recovered. H3K56ac can interfere with this recovery (orange dashed arrow) by dilution of the methylation signal due to increased turnover of histones, thus decreasing transcription from replicated regions. Upon replication stress (e.g., HU), the DNA replication checkpoint interferes with the methylation feedback by phosphorylating PAF1C and depleting Pol II from replicated DNA. In addition, the checkpoint can function through stabilization of the H3K56ac signal.

been extensively studied in the context of transcription (Buratowski and Kim, 2010). H3K4 is methylated by COMPASS, which is recruited to the DNA by the transcription elongation complex PAF1C (Krogan et al., 2003; Ng et al., 2003). COMPASS and PAF1C emerged from our *in silico* screen of 1,484 mutants as main effectors of expression homeostasis. Consistently, replicated genes show reduced levels of the transcription-activating H3K4me3 mark and an increase in the inhibitory H3K4me2 mark close to the transcription start site.

H3K4me3 forms a positive feedback loop with gene expression: it is deposited through multiple cycles of transcription (Soares et al., 2017) and leads, in turn, to increased transcription, both by directly promoting expression and by replacing the inhibitory H3K4me2 mark (Buratowski and Kim, 2010; Kim and Buratowski, 2009; Lauberth et al., 2013). As newly synthesized histones used for wrapping replicated genes are not methylated (Benson et al., 2006), achieving maximal expression of these genes likely entails recovery of pre-replication H3K4me. Interfering with this process, or slowing it down, may therefore suppress transcription from replicated DNA.

The pattern of H3K56ac remains intact in *paf1Δ* cells, even though this mutation reduces H3K4me (Krogan et al., 2003) and partially compromises buffering. This leads us to favor a model in which H3K56ac suppresses transcription from replicated regions by slowing down the post-replication recovery of H3K4me3. This could be due to direct interference with PAF1C or COMPASS activity. Alternatively, it could be a consequence of the accelerated turnover of H3K56ac-labeled histones, which promotes the dilution of histone marks added during transcription (Kaplan et al., 2008; Rufiange et al., 2007). Of note, turnover-dependent dilution would affect not only H3K4me3 but also other transcription-associated modifications, such as H3K36me3 and H3K79me3, which similarly showed delayed post-replication recovery (Figure S2B; Bar-Ziv et al., 2016). The partial loss of buffering observed in cells deleted of COMPASS subunits may be explained by additive effects exerted by H3K36me3 and H3K79me3. These effects may also account for the full loss of buffering upon deletion of *RTF1*, the PAF1C subunit that mediates its chromatin-modifying roles (Mayekar et al., 2013). Why deletion of *PAF1* itself leads only to partial loss of buffering is not clear and may reflect the severely prolonged replication and delayed transcription in this mutant, which is partially rescued by deletion of *SET1*.

Notably, following HU treatment buffering becomes fully dependent on the replication checkpoint. This additional requirement may reflect the challenge of maintaining buffering for an extended period in which cells are arrested with their genome partially replicated. Indeed, during normal S phase, residual expression (~10% increase in mRNA levels and ~30% in mRNA synthesis rate) of replicated genes is observed (Voichek et al., 2016). Within our dynamic framework, this residual expression may be amplified during extended S phase, requiring further attenuation of gene expression.

Upon HU exposure, the replication checkpoint phosphorylates Paf1, which leads to Pol II eviction and degradation (Poli et al., 2016). Depletion of Pol II from replicated regions not only reduces transcription but is also expected to further diminish the efficiency of post-replication recovery of H3K4me (Soares et al., 2017). Together, the two can contribute to the buffering mechanism. In addition, the checkpoint stabilizes H3K56ac during extended S phase, possibly providing another arm through which it contributes to buffering (Edenberg et al., 2014; Thaminy et al., 2007). Finally, the checkpoint kinase Rad53 may function through yet another process, as deletion of Rad53 similarly results in loss of homeostasis but at a significant delay relative to deletion of the checkpoint sensor Mec1.

Taken together, we propose that buffering expression from replicated genes depends on the dynamic process by which epigenetic modifications are recovered following replication. It is often the case that epigenetic marks form feedback loops with gene expression, being both a consequence and a cause of gene transcription. These feedback circuits present a fertile ground for regulatory controls. We therefore propose a mechanism that exemplifies these possibilities (Figure 7): H3K56ac

and PAF1C interfere with the positive feedback loop controlling H3K4 methylation. The post-replication recovery of H3K4 methylation can be controlled and adjusted depending on external requirements, providing the ability to buffer gene expression against replication-dependent dosage imbalance. The full reliance on a functional replication checkpoint to maintain this buffering during replication stress not only defines a new role for the checkpoint but also suggests the importance of this buffering for maintaining genome integrity.

## STAR★METHODS

Detailed methods are provided in the online version of this paper and include the following:

- KEY RESOURCES TABLE
- CONTACT FOR REAGENT AND RESOURCE SHARING
- EXPERIMENTAL MODEL AND SUBJECT DETAILS
  - Yeast Strains and Genomic Manipulations
- METHOD DETAILS
  - CRISPR/Cas9 Genetic Manipulations
  - Cell-cycle synchronization and release to HU or YPD
  - DNA extraction and library preparation
  - RNA extraction
  - RNA sequencing
  - ChIP-seq
  - Whole Cell Extracts and Immunoblotting
- QUANTIFICATION AND STATISTICAL ANALYSES
  - Processing and analysis of RNA-seq data
  - Processing and analysis of ChIP-seq and genomic DNA data
  - Estimation of expression from replicated regions
  - Estimation of Pol II, H3K4me2 or H3K4me3 on replicated regions
- DATA AND SOFTWARE AVAILABILITY

## SUPPLEMENTAL INFORMATION

Supplemental Information includes five figures and two tables and can be found with this article online at https://doi.org/10.1016/j.molcel.2018.05.015.

## ACKNOWLEDGMENTS

We thank Maria Pia Longhese and Stephen Elledge for sharing their strains, Alain Verreault for the H3K56ac antibody, and Ido Amit for the Tn5 transposase. We thank Miri Carmi for technical assistance. We thank Daphna Joseph-Strauss and Nir Friedman for assistance with the RNA sequencing (RNA-seq) protocol. This work was supported by the European Research Council (ERC, 338660) and the Minerva Center (AZ 57 46 9407 65).

## AUTHOR CONTRIBUTIONS

Y.V., K.M., and N.B. conceived the study and designed experiments; Y.V., K.M., Y.G., R.B.-Z., D.L.S., and R.S. performed experiments; Y.V. and K.M. analyzed the data; Y.V., K.M., and N.B. wrote the manuscript; and N.B. supervised the research.

## DECLARATION OF INTERESTS

The authors declare no competing interests.

Received: December 26, 2017
Revised: March 22, 2018
Accepted: May 11, 2018
Published: June 14, 2018

## REFERENCES

Bar-Ziv, R., Voichek, Y., and Barkai, N. (2016). Chromatin dynamics during DNA replication. Genome Res. *26*, 1245–1256.

Bartek, J., Lukas, C., and Lukas, J. (2004). Checking on DNA damage in S phase. Nat. Rev. Mol. Cell Biol. *5*, 792–804.

Beckwith, J.R., Signer, E.R., and Epstein, W. (1966). Transposition of the Lac region of E. coli. Cold Spring Harb. Symp. Quant. Biol. *31*, 393–401.

Benson, L.J., Gu, Y., Yakovleva, T., Tong, K., Barrows, C., Strack, C.L., Cook, R.G., Mizzen, C.A., and Annunziato, A.T. (2006). Modifications of H3 and H4 during chromatin replication, nucleosome assembly, and histone exchange. J. Biol. Chem. *281*, 9287–9296.

Blecher-Gonen, R., Barnett-Itzhaki, Z., Jaitin, D., Amann-Zalcenstein, D., Lara-Astiaso, D., and Amit, I. (2013). High-throughput chromatin immunoprecipitation for genome-wide mapping of in vivo protein-DNA interactions and epigenomic states. Nat. Protoc. *8*, 539–554.

Buratowski, S., and Kim, T. (2010). The role of cotranscriptional histone methylations. Cold Spring Harb. Symp. Quant. Biol. *75*, 95–102.

Celic, I., Masumoto, H., Griffith, W.P., Meluh, P., Cotter, R.J., Boeke, J.D., and Verreault, A. (2006). The sirtuins hst3 and Hst4p preserve genome integrity by controlling histone h3 lysine 56 deacetylation. Curr. Biol. *16*, 1280–1289.

Chabes, A., Domkin, V., and Thelander, L. (1999). Yeast Sml1, a protein inhibitor of ribonucleotide reductase. J. Biol. Chem. *274*, 36679–36683.

Chandler, M.G., and Pritchard, R.H. (1975). The effect of gene concentration and relative gene dosage on gene output in Escherichia coli. Mol. Gen. Genet. *138*, 127–141.

Dermody, J.L., and Buratowski, S. (2010). Leo1 subunit of the yeast paf1 complex binds RNA and contributes to complex recruitment. J. Biol. Chem. *285*, 33671–33679.

DiCarlo, J.E., Norville, J.E., Mali, P., Rios, X., Aach, J., and Church, G.M. (2013). Genome engineering in Saccharomyces cerevisiae using CRISPR-Cas systems. Nucleic Acids Res. *41*, 4336–4343.

Dover, J., Schneider, J., Tawiah-Boateng, M.A., Wood, A., Dean, K., Johnston, M., and Shilatifard, A. (2002). Methylation of histone H3 by COMPASS requires ubiquitination of histone H2B by Rad6. J. Biol. Chem. *277*, 28368–28371.

Driscoll, R., Hudson, A., and Jackson, S.P. (2007). Yeast Rtt109 promotes genome stability by acetylating histone H3 on lysine 56. Science *315*, 649–652.

Edenberg, E.R., Vashisht, A.A., Topacio, B.R., Wohlschlegel, J.A., and Toczyski, D.P. (2014). Hst3 is turned over by a replication stress-responsive SCF(Cdc4) phospho-degron. Proc. Natl. Acad. Sci. USA *111*, 5962–5967.

Elliott, S.G., and McLaughlin, C.S. (1978). Rate of macromolecular synthesis through the cell cycle of the yeast Saccharomyces cerevisiae. Proc. Natl. Acad. Sci. USA *75*, 4384–4388.

Gasch, A.P., Spellman, P.T., Kao, C.M., Carmel-Harel, O., Eisen, M.B., Storz, G., Botstein, D., and Brown, P.O. (2000). Genomic expression programs in the response of yeast cells to environmental changes. Mol. Biol. Cell *11*, 4241–4257.

Gasch, A.P., Huang, M., Metzner, S., Botstein, D., Elledge, S.J., and Brown, P.O. (2001). Genomic expression responses to DNA-damaging agents and the regulatory role of the yeast ATR homolog Mec1p. Mol. Biol. Cell *12*, 2987–3003.

Gietz, R.D., Schiestl, R.H., Willems, A.R., and Woods, R.A. (1995). Studies on the transformation of intact yeast cells by the LiAC/SS-DNA/PEG procedure. Yeast *11*, 355–360.

Han, J., Zhou, H., Horazdovsky, B., Zhang, K., Xu, R.-M., and Zhang, Z. (2007a). Rtt109 acetylates histone H3 lysine 56 and functions in DNA replication. Science *315*, 653–655.

Han, J., Zhou, H., Li, Z., Xu, R.-M., and Zhang, Z. (2007b). The Rtt109-Vps75 histone acetyltransferase complex acetylates non-nucleosomal histone H3. J. Biol. Chem. *282*, 14158–14164.

Hanna, J.S., Kroll, E.S., Lundblad, V., and Spencer, F.A. (2001). Saccharomyces cerevisiae CTF18 and CTF4 are required for sister chromatid cohesion. Mol. Cell. Biol. *21*, 3144–3158.

Ihmels, J., Friedlander, G., Bergmann, S., Sarig, O., Ziv, Y., and Barkai, N. (2002). Revealing modular organization in the yeast transcriptional network. Nat. Genet. *31*, 370–377.

Kaplan, T., Liu, C.L., Erkmann, J.A., Holik, J., Grunstein, M., Kaufman, P.D., Friedman, N., and Rando, O.J. (2008). Cell cycle- and chaperone-mediated regulation of H3K56ac incorporation in yeast. PLoS Genet. *4*, e1000270.

Kemmeren, P., Sameith, K., van de Pasch, L.A.L., Benschop, J.J., Lenstra, T.L., Margaritis, T., O'Duibhir, E., Apweiler, E., van Wageningen, S., Ko, C.W., et al. (2014). Large-scale genetic perturbations reveal regulatory networks and an abundance of gene-specific repressors. Cell *157*, 740–752.

Kim, T., and Buratowski, S. (2009). Dimethylation of H3K4 by Set1 recruits the Set3 histone deacetylase complex to 5′ transcribed regions. Cell *137*, 259–272.

Kivioja, T., Vähärautio, A., Karlsson, K., Bonke, M., Enge, M., Linnarsson, S., and Taipale, J. (2011). Counting absolute numbers of molecules using unique molecular identifiers. Nat. Methods *9*, 72–74.

Koç, A., Wheeler, L.J., Mathews, C.K., and Merrill, G.F. (2004). Hydroxyurea arrests DNA replication by a mechanism that preserves basal dNTP pools. J. Biol. Chem. *279*, 223–230.

Krogan, N.J., Kim, M., Ahn, S.H., Zhong, G., Kobor, M.S., Cagney, G., Emili, A., Shilatifard, A., Buratowski, S., and Greenblatt, J.F. (2002). RNA polymerase II elongation factors of Saccharomyces cerevisiae: a targeted proteomics approach. Mol. Cell. Biol. *22*, 6979–6992.

Krogan, N.J., Dover, J., Wood, A., Schneider, J., Heidt, J., Boateng, M.A., Dean, K., Ryan, O.W., Golshani, A., Johnston, M., et al. (2003). The Paf1 complex is required for histone H3 methylation by COMPASS and Dot1p: linking transcriptional elongation to histone methylation. Mol. Cell *11*, 721–729.

Langmead, B., Trapnell, C., Pop, M., and Salzberg, S.L. (2009). Ultrafast and memory-efficient alignment of short DNA sequences to the human genome. Genome Biol. *10*, R25.

Laribee, R.N., Krogan, N.J., Xiao, T., Shibata, Y., Hughes, T.R., Greenblatt, J.F., and Strahl, B.D. (2005). BUR kinase selectively regulates H3 K4 trimethylation and H2B ubiquitylation through recruitment of the PAF elongation complex. Curr. Biol. *15*, 1487–1493.

Lauberth, S.M., Nakayama, T., Wu, X., Ferris, A.L., Tang, Z., Hughes, S.H., and Roeder, R.G. (2013). H3K4me3 interactions with TAF3 regulate preinitiation complex assembly and selective gene activation. Cell *152*, 1021–1036.

Lenstra, T.L., Benschop, J.J., Kim, T., Schulze, J.M., Brabers, N.A.C.H., Margaritis, T., van de Pasch, L.A.L., van Heesch, S.A.A.C., Brok, M.O., Groot Koerkamp, M.J.A., et al. (2011). The specificity and topology of chromatin interaction pathways in yeast. Mol. Cell *42*, 536–549.

Longhese, M.P., Paciotti, V., Neecke, H., and Lucchini, G. (2000). Checkpoint proteins influence telomeric silencing and length maintenance in budding yeast. Genetics *155*, 1577–1591.

Mans, R., van Rossum, H.M., Wijsman, M., Backx, A., Kuijpers, N.G.A., van den Broek, M., Daran-Lapujade, P., Pronk, J.T., van Maris, A.J.A., and Daran, J.-M.G. (2015). CRISPR/Cas9: a molecular Swiss army knife for simultaneous introduction of multiple genetic modifications in Saccharomyces cerevisiae. FEMS Yeast Res. *15*, fov004.

Mayekar, M.K., Gardner, R.G., and Arndt, K.M. (2013). The recruitment of the Saccharomyces cerevisiae Paf1 complex to active genes requires a domain of Rtf1 that directly interacts with the Spt4-Spt5 complex. Mol. Cell. Biol. *33*, 3259–3273.

Miller, T., Krogan, N.J., Dover, J., Erdjument-Bromage, H., Tempst, P., Johnston, M., Greenblatt, J.F., and Shilatifard, A. (2001). COMPASS: a complex of proteins associated with a trithorax-related SET domain protein. Proc. Natl. Acad. Sci. USA *98*, 12902–12907.

Miller, C., Schwalb, B., Maier, K., Schulz, D., Dümcke, S., Zacher, B., Mayer, A., Sydow, J., Marcinowski, L., Dölken, L., et al. (2011). Dynamic transcriptome analysis measures rates of mRNA synthesis and decay in yeast. Mol. Syst. Biol. *7*, 458.

Mirkin, E.V., and Mirkin, S.M. (2007). Replication fork stalling at natural impediments. Microbiol. Mol. Biol. Rev. *71*, 13–35.

Mulder, K.W., Winkler, G.S., and Timmers, H.T.M. (2005). DNA damage and replication stress induced transcription of RNR genes is dependent on the Ccr4-Not complex. Nucleic Acids Res. *33*, 6384–6392.

Naylor, M.L., Li, J.M., Osborn, A.J., and Elledge, S.J. (2009). Mrc1 phosphorylation in response to DNA replication stress is required for Mec1 accumulation at the stalled fork. Proc. Natl. Acad. Sci. USA *106*, 12765–12770.

Ng, H.H., Robert, F., Young, R.A., and Struhl, K. (2003). Targeted recruitment of Set1 histone methylase by elongating Pol II provides a localized mark and memory of recent transcriptional activity. Mol. Cell *11*, 709–719.

Nieduszynski, C.A., Hiraga, S., Ak, P., Benham, C.J., and Donaldson, A.D. (2007). OriDB: a DNA replication origin database. Nucleic Acids Res. *35*, D40–D46.

Osborn, A.J., and Elledge, S.J. (2003). Mrc1 is a replication fork component whose phosphorylation in response to DNA replication stress activates Rad53. Genes Dev. *17*, 1755–1767.

Paciotti, V., Clerici, M., Scotti, M., Lucchini, G., and Longhese, M.P. (2001). Characterization of mec1 kinase-deficient mutants and of new hypomorphic mec1 alleles impairing subsets of the DNA damage response pathway. Mol. Cell. Biol. *21*, 3913–3925.

Padovan-Merhar, O., Nair, G.P., Biaesch, A.G., Mayer, A., Scarfone, S., Foley, S.W., Wu, A.R., Churchman, L.S., Singh, A., and Raj, A. (2015). Single mammalian cells compensate for differences in cellular volume and DNA copy number through independent global transcriptional mechanisms. Mol. Cell *58*, 339–352.

Pelechano, V., Wei, W., and Steinmetz, L.M. (2013). Extensive transcriptional heterogeneity revealed by isoform profiling. Nature *497*, 127–131.

Poli, J., Gerhold, C.-B., Tosi, A., Hustedt, N., Seeber, A., Sack, R., Herzog, F., Pasero, P., Shimada, K., Hopfner, K.-P., and Gasser, S.M. (2016). Mec1, INO80, and the PAF1 complex cooperate to limit transcription replication conflicts through RNAPII removal during replication stress. Genes Dev. *30*, 337–354.

Radman-Livaja, M., Liu, C.L., Friedman, N., Schreiber, S.L., and Rando, O.J. (2010). Replication and active demethylation represent partially overlapping mechanisms for erasure of H3K4me3 in budding yeast. PLoS Genet. *6*, e1000837.

Rufiange, A., Jacques, P.-E., Bhat, W., Robert, F., and Nourani, A. (2007). Genome-wide replication-independent histone H3 exchange occurs predominantly at promoters and implicates H3 K56 acetylation and Asf1. Mol. Cell *27*, 393–405.

Santos-Rosa, H., Schneider, R., Bannister, A.J., Sherriff, J., Bernstein, B.E., Emre, N.C.T., Schreiber, S.L., Mellor, J., and Kouzarides, T. (2002). Active genes are tri-methylated at K4 of histone H3. Nature *419*, 407–411.

Schmid, M.B., and Roth, J.R. (1987). Gene location affects expression level in Salmonella typhimurium. J. Bacteriol. *169*, 2872–2875.

Simic, R., Lindstrom, D.L., Tran, H.G., Roinick, K.L., Costa, P.J., Johnson, A.D., Hartzog, G.A., and Arndt, K.M. (2003). Chromatin remodeling protein Chd1 interacts with transcription elongation factors and localizes to transcribed genes. EMBO J. *22*, 1846–1856.

Slager, J., Kjos, M., Attaiech, L., and Veening, J.-W. (2014). Antibiotic-induced replication stress triggers bacterial competence by increasing gene dosage near the origin. Cell *157*, 395–406.

Soares, L.M., He, P.C., Chun, Y., Suh, H., Kim, T., and Buratowski, S. (2017). Determinants of histone H3K4 methylation patterns. Mol. Cell *68*, 773–785.e6.

Sobel, R.E., Cook, R.G., Perry, C.A., Annunziato, A.T., and Allis, C.D. (1995). Conservation of deposition-related acetylation sites in newly synthesized histones H3 and H4. Proc. Natl. Acad. Sci. USA *92*, 1237–1241.

Tercero, J.A., and Diffley, J.F. (2001). Regulation of DNA replication fork progression through damaged DNA by the Mec1/Rad53 checkpoint. Nature *412*, 553–557.

Thaminy, S., Newcomb, B., Kim, J., Gatbonton, T., Foss, E., Simon, J., and Bedalov, A. (2007). Hst3 is regulated by Mec1-dependent proteolysis and controls the S phase checkpoint and sister chromatid cohesion by deacetylating histone H3 at lysine 56. J. Biol. Chem. *282*, 37805–37814.

Torres, E.M., Sokolsky, T., Tucker, C.M., Chan, L.Y., Boselli, M., Dunham, M.J., and Amon, A. (2007). Effects of aneuploidy on cellular physiology and cell division in haploid yeast. Science *317*, 916–924.

van den Ent, F., and Löwe, J. (2006). RF cloning: a restriction-free method for inserting target genes into plasmids. J. Biochem. Biophys. Methods *67*, 67–74.

Voichek, Y., Bar-Ziv, R., and Barkai, N. (2016). Expression homeostasis during DNA replication. Science *351*, 1087–1090.

Xu, Y., Bernecky, C., Lee, C.-T., Maier, K.C., Schwalb, B., Tegunov, D., Plitzko, J.M., Urlaub, H., and Cramer, P. (2017). Architecture of the RNA polymerase II-Paf1C-TFIIS transcription elongation complex. Nat. Commun. *8*, 15741.

Yabuki, N., Terashima, H., and Kitada, K. (2002). Mapping of early firing origins on a replication profile of budding yeast. Genes Cells *7*, 781–789.

Zegerman, P., and Diffley, J.F.X. (2009). DNA replication as a target of the DNA damage checkpoint. DNA Repair (Amst.) *8*, 1077–1088.

Zhou, B.B., and Elledge, S.J. (2000). The DNA damage response: putting checkpoints in perspective. Nature *408*, 433–439.

# STAR★METHODS

## KEY RESOURCES TABLE

| REAGENT or RESOURCE | SOURCE | IDENTIFIER |
|---|---|---|
| Antibodies | | |
| Rabbit polyclonal anti-histone H3 (acetylated K56) | Alain Verreault | N/A |
| Rabbit polyclonal anti-histone H3 (acetylated K56) | Active Motif | Cat#39281am; RRID: AB_2661786 |
| Mouse monoclonal anti-Pol II (8WG16) | Enzo | Cat#ENZ-ABS132 |
| Mouse monoclonal anti-Pol II (8WG16) | Enzo | Cat#ENZ-ABS132A |
| Mouse monoclonal anti-histone H3 (tri-methyl K4) | Abcam | Cat#ab1012; RRID: AB_442796 |
| Rabbit monoclonal anti-histone H3 (di-methyl K4) | Abcam | Cat#ab32356; RRID: AB_732924 |
| Mouse monoclonal anti-Actin (Clone: C4) | MP Biomedicals | Cat#0869100; |
| Anti-rabbit IgG, HRP-linked antibody | Cell Signaling Technology | Cat#CST-7074P2 |
| Anti-mouse IgG, HRP-linked antibody | Cell Signaling Technology | Cat#CST-7076P2 |
| Chemicals, Peptides, and Recombinant Proteins | | |
| Y2016 Yeast Mating Factor Alpha (α-factor) | US Biological Life Sciences | Cat#59401-28-4 |
| Hydroxyurea (HU) | Bio Basic | Cat#HB0528 |
| Protease Inhibitor Cocktail Set IV | Calbiochem | Cat#539136 |
| Tn5 transposase (Tn5, hyperactive variant) | Ido Amit | N/A |
| Critical Commercial Assays | | |
| Total RNA Isolation Nucleospin 96 | Macherey-Nagel | Cat#740709 |
| HiYield Plasmid Mini Kit | RBC Bioscience | Cat#YPD100 |
| Dynabeads Protein G for Immunoprecipitation | Invitrogen | Cat#10003D |
| Pierce 660nm Protein Assay Reagent | Thermo Fisher Scientific | Cat#22660 |
| Ionic Detergent Compatibility Reagent (IDCR) for Pierce 660nm Protein Assay Reagent | Thermo Fisher Scientific | Cat#22663 |
| EZ-ECL | Biological Industries | Cat#20-500-120 |
| Deposited Data | | |
| RNA-seq, ChIP-seq and DNA-seq data | This study | SRA database, BioProject PRJNA438153 |
| Yeast reference genome version R64-1-1 | SGD | https://downloads.yeastgenome.org/sequence/S288C_reference/genome_releases/S288C_reference_genome_R64-1-1_20110203.tgz |
| Gel images | This study | https://doi.org/10.17632/zw945my9v4.1 |
| Experimental Models: Organisms/Strains | | |
| mec1-100 (W303 MATa, ade2-1 can1-100 his3-11,15 leu2-3,112 trp1-1 ura3 sml1Δ::KanMX4 mec1-100::LEU2::mec1Δ) | Paciotti et al., 2001 | N/A |
| mec1-101 (W303 MATa, ade2-1 can1-100 his3-11,15 leu2-3,112 trp1-1 ura3 sml1Δ::KanMX4 mec1-101::LEU2::mec1Δ) | Paciotti et al., 2001 | N/A |
| mec1Δsml1Δ (W303 MATa, ade2-1 can1-100 his3-11,15 leu2-3,112 trp1-1 ura3 mec1Δ::HIS3 sml1Δ::KanMX4) | Longhese et al., 2000 | N/A |
| mrc1Δ (BY4741 MATa, his3-1, leu2-0, met15-0, ura3-0, mrc1::KanMX) | This study | N/A |
| mrc1-AQ (W303 MATa, Y2298 \| trp1-1 ura3-1 his3-11,15 leu2-3,112 ade2-1 can1-100 HIS::mrcIAQ MYC13) | Osborn and Elledge, 2003 | N/A |

(*Continued on next page*)

*Continued*

| REAGENT or RESOURCE | SOURCE | IDENTIFIER |
|---|---|---|
| mrc1-C14 (W303 MATa, Y2544 \|trp1-1 ura3-1 his3-11,15 leu2-3,112 ade2-1 can1-100 KANMX::mrc1-C14-MYC13) | Naylor et al., 2009 | N/A |
| MRC1-myc (W303 MATa, Y1134 \| trp1-1 ura3-1 his3-11,15 leu2-3,112 ade2-1 can1-100 HIS::MRC1-MYC5) | Naylor et al., 2009 | N/A |
| WT (BY4741 MATa, his3-1, leu2-0, met15-0, ura3-0) | Euroscarf | N/A |
| tos4Δ (BY4741 MATa, his3-1, leu2-0, met15-0, ura3-0, tos4::KanMX) | Voichek et al., 2016 | N/A |
| sml1Δ (BY4741 MATa, his3-1, leu2-0, met15-0, ura3-0, sml1::KanMX) | This study | N/A |
| mec1Δsml1Δ (BY4741 MATa, his3-1, leu2-0, met15-0, ura3-0, sml1::KanMX, mec1:: hphNT1) | This study | N/A |
| rad53Δsml1Δ (BY4741 MATa, his3-1, leu2-0, met15-0, ura3-0, sml1::KanMX, rad53:: hphNT1) | This study | N/A |
| rtt109Δ (BY4741 MATa, his3-1, leu2-0, met15-0, ura3-0, rtt109::KanMX) | Voichek et al., 2016 | N/A |
| rtt109Δtos4Δ (BY4741 MATa, his3-1, leu2-0, met15-0, ura3-0, rtt109::KanMX, tos4::HYG) | Voichek et al., 2016 | N/A |
| cac1Δ (BY4741 MATa, his3-1, leu2-0, met15-0, ura3-0, cac1::KanMX) | This study | N/A |
| rtt106Δ (BY4741 MATa, his3-1, leu2-0, met15-0, ura3-0, rtt106::KanMX) | This study | N/A |
| ckb1Δ (BY4741 MATa, his3-1, leu2-0, met15-0, ura3-0, ckb1::KanMX) | This study | N/A |
| ckb2Δ (BY4741 MATa, his3-1, leu2-0, met15-0, ura3-0, ckb2::KanMX) | This study | N/A |
| clb5Δ (BY4741 MATa, his3-1, leu2-0, met15-0, ura3-0, clb5::KanMX) | This study | N/A |
| clb6Δ (BY4741 MATa, his3-1, leu2-0, met15-0, ura3-0, clb6::KanMX) | This study | N/A |
| vps75Δ (BY4741 MATa, his3-1, leu2-0, met15-0, ura3-0, vps75::KanMX) | This study | N/A |
| asf1Δ (BY4741 MATa, his3-1, leu2-0, met15-0, ura3-0, asf1::KanMX) | Voichek et al., 2016 | N/A |
| dun1Δ (BY4741 MATa, his3-1, leu2-0, met15-0, ura3-0, dun1::KanMX) | This study | N/A |
| med15Δ (BY4741 MATa, his3-1, leu2-0, met15-0, ura3-0, med15::KanMX) | This study | N/A |
| rtr1Δ (BY4741 MATa, his3-1, leu2-0, met15-0, ura3-0, rtr1::KanMX) | This study | N/A |
| hst3Δ (BY4741 MATa, his3-1, leu2-0, met15-0, ura3-0, hst3::KanMX) | This study | N/A |
| hst4Δ (BY4741 MATa, his3-1, leu2-0, met15-0, ura3-0, hst4::KanMX) | This study | N/A |
| sus1Δ (BY4741 MATa, his3-1, leu2-0, met15-0, ura3-0, sus1::KanMX) | This study | N/A |
| bur2Δ (BY4741 MATa, his3-1, leu2-0, met15-0, ura3-0, bur2::KanMX) | This study | N/A |
| ctr9Δ (BY4741 MATa, his3-1, leu2-0, met15-0, ura3-0, ctr9::KanMX) | This study | N/A |
| paf1Δ (BY4741 MATa, his3-1, leu2-0, met15-0, ura3-0, paf1::KanMX) | This study | N/A |

(*Continued on next page*)

*Continued*

| REAGENT or RESOURCE | SOURCE | IDENTIFIER |
|---|---|---|
| rbp9Δ (BY4741 MATa, his3-1, leu2-0, met15-0, ura3-0, rpb9::KanMX) | This study | N/A |
| ssn3Δ (BY4741 MATa, his3-1, leu2-0, met15-0, ura3-0, ssn3::KanMX) | This study | N/A |
| ctk1Δ (BY4741 MATa, his3-1, leu2-0, met15-0, ura3-0, ctk1::KanMX) | This study | N/A |
| H3K56Q (BY4741 MATa, his3-1, leu2-0, met15-0, ura3-0,HHT1[56Lys- > Gln],HHT2[56Lys- > Gln]) | This study | N/A |
| H3K56A (BY4741 MATa, his3-1, leu2-0, met15-0, ura3-0,HHT1[56Lys- > Ala],HHT2[56Lys- > Ala]) | This study | N/A |
| H3K56R (BY4741 MATa, his3-1, leu2-0, met15-0, ura3-0,HHT1[56Lys- > Arg],HHT2[56Lys- > Arg]) | This study | N/A |
| set1Δ (BY4741 MATa, his3-1, leu2-0, met15-0, ura3-0, set1::KanMX) | This study | N/A |
| set2Δ (BY4741 MATa, his3-1, leu2-0, met15-0, ura3-0, set2::KanMX) | This study | N/A |
| swd1Δ (BY4741 MATa, his3-1, leu2-0, met15-0, ura3-0, swd1::KanMX) | This study | N/A |
| swd3Δ (BY4741 MATa, his3-1, leu2-0, met15-0, ura3-0, swd3::KanMX) | This study | N/A |
| clb5Δ (BY4741 MATa, his3-1, leu2-0, met15-0, ura3-0, clb5::KanMX) | This study | N/A |
| ctf8Δ (BY4741 MATa, his3-1, leu2-0, met15-0, ura3-0, ctf8::KanMX) | This study | N/A |
| ctf18Δ (BY4741 MATa, his3-1, leu2-0, met15-0, ura3-0, ctf18::KanMX) | This study | N/A |
| swi3Δ (BY4741 MATa, his3-1, leu2-0, met15-0, ura3-0, swi3::KanMX) | This study | N/A |
| plm2Δ (BY4741 MATa, his3-1, leu2-0, met15-0, ura3-0, plm2::KanMX) | This study | N/A |
| hst1Δ (BY4741 MATa, his3-1, leu2-0, met15-0, ura3-0, hst1::KanMX) | This study | N/A |
| ubp8Δ (BY4741 MATa, his3-1, leu2-0, met15-0, ura3-0, ubp8::KanMX) | This study | N/A |
| hos4Δ (BY4741 MATa, his3-1, leu2-0, met15-0, ura3-0, hos4::KanMX) | This study | N/A |
| sum1Δ (BY4741 MATa, his3-1, leu2-0, met15-0, ura3-0, sum1::KanMX) | This study | N/A |
| upf3Δ (BY4741 MATa, his3-1, leu2-0, met15-0, ura3-0, upf3::KanMX) | This study | N/A |
| npt1Δ (BY4741 MATa, his3-1, leu2-0, met15-0, ura3-0, npt1::KanMX) | This study | N/A |
| cha4Δ (BY4741 MATa, his3-1, leu2-0, met15-0, ura3-0, cha4::KanMX) | This study | N/A |
| rnr4Δ (BY4741 MATa, his3-1, leu2-0, met15-0, ura3-0, rnr4::KanMX) | This study | N/A |
| swi6Δ (BY4741 MATa, his3-1, leu2-0, met15-0, ura3-0, swi6::D) | This study | N/A |
| Hst3Δ97 (BY4741 MATa, his3-1, leu2-0, met15-0, ura3-0, hst3C97::KanMX) | This study | N/A |
| rtf1Δ (BY4741 MATa, his3-1, leu2-0, met15-0, ura3-0, rtf1::KanMX) | This study | N/A |

(*Continued on next page*)

*Continued*

| REAGENT or RESOURCE | SOURCE | IDENTIFIER |
|---|---|---|
| paf1Δset1Δ (BY4741 MATa, his3-1, leu2-0, met15-0, ura3-0, paf1::hphMX6, set1::KanMX) | This study | N/A |
| rtf1Δ (BY4741 MATa, his3-1, leu2-0, met15-0, ura3-0, rtf1::KanMX) | This study | N/A |
| cdc73Δ (BY4741 MATa, his3-1, leu2-0, met15-0, ura3-0, cdc73::KanMX) | This study | N/A |
| leo1Δ (BY4741 MATa, his3-1, leu2-0, met15-0, ura3-0, leo1::KanMX) | This study | N/A |
| ies5Δ (BY4741 MATa, his3-1, leu2-0, met15-0, ura3-0, ies5::KanMX) | This study | N/A |
| nhp10Δ (BY4741 MATa, his3-1, leu2-0, met15-0, ura3-0, nhp10::KanMX) | This study | N/A |
| ies2Δ (BY4741 MATa, his3-1, leu2-0, met15-0, ura3-0, ies2::KanMX) | This study | N/A |
| rtt109Δset1Δ (BY4741 MATa, his3-1, leu2-0, met15-0, ura3-0, rtt109::hphMX6, set1::KanMX) | This study | N/A |
| rtt109Δmec1Δsml1Δ (BY4741 MATa, his3-1, leu2-0, met15-0, ura3-0, rtt109::KanMX, mec1::hphMX6, sml1::D) | This study | N/A |
| rtt109Δrad53Δsml1Δ (BY4741 MATa, his3-1, leu2-0, met15-0, ura3-0, rtt109::KanMX, rad53::hphMX6, sml1::D) | This study | N/A |
| Oligonucleotides | | |
| Primers used for strain creation | This study | See Table S2 |
| Recombinant DNA | | |
| pBS7 | Yeast Resource Center | N/A |
| pAG32 | AddGene | Cat#35122 |
| pYM24 | Euroscarf | Cat#P30236 |
| pMEL13 | Mans et al., 2015 | N/A |
| P416 | DiCarlo et al., 2013 | N/A |
| Software and Algorithms | | |
| bowtie | Langmead et al., 2009 | N/A |
| Other | | |
| *Saccharomyces* Genome Deletion Project | Stanford Genome Technology Center | http://www-sequence.stanford.edu/group/yeast_deletion_project/usites.html |

## CONTACT FOR REAGENT AND RESOURCE SHARING

Further information and requests for resources and reagents should be directed to and will be fulfilled by the lead contact, Naama Barkai (naama.barkai@weizmann.ac.il).

## EXPERIMENTAL MODEL AND SUBJECT DETAILS

### Yeast Strains and Genomic Manipulations

All strains used in this study are described in the Key Resources table. Deletion strains were derived from BY4741 *MATa his3-Δ1 leu2-Δ0 lys2-Δ0 met15-Δ0 ura3-Δ0* using the LiAc/SS DNA/PEG method described by Gietz et al. (1995): stationary cells were inoculated into fresh YPD and allowed to grow so that they completed two cell divisions. Cells were then washed with DDW and subsequently with LiAc 100mM. Cells were then resuspended in transformation mix (33% $PEG_{3350}$, 100mM LiAc, single stranded salmon sperm DNA and the DNA intended for transformation). The cells were incubated at 30°C for 30 minutes followed by a 30 minute heat shock (42°C). When transformed with antibiotic markers, cells were plated on YPD agar plates for overnight recovery and then replicated to the appropriate selection plates.

In single deletion strains except for *swi6Δ*, the gene deleted was replaced with the KanMX cassette (geneD::KanMX) amplified from the plasmid pBS7 (Yeast Resource Center) using UPTAG and DNTAG primers as described in the Yeast Deletion Project (http://www-sequence.stanford.edu/group/yeast_deletion_project/usites.html). The deletion was then validated with primers A, B, and kanB as described in the project overview.

*swi6Δ*, H3K56Q, H3K56A and H3K56R were created using CRISPR/Cas9 genetic manipulations as described below.

*sml1Δ* was created as described above and used as a background strain for generation of *mec1Δsml1Δ and rad53Δsml1Δ*. *MEC1* and *RAD53* were replaced with the hygromycin B cassette (*mec1/rad53*:: hphNT1) amplified from plasmid pYM24 using primers mec1 F and mec1 R for *mec1Δsml1Δ* and primers rad53 F and rad53 R for *rad53Δsml1Δ* (Table S2).The deletions were verified by DNA sequencing.

*set1Δ* was created as described above and used as a background strain for generation of *paf1Δset1Δ and rtt109Δset1Δ*. *PAF1* and *RTT109* were each replaced with the hygromycin B cassette (*paf1*::hphMX6) amplified from plasmid pAG32 using primers Paf1 For and Paf1 Rev and Rtt109 F and Rtt109 R, respectively (Table S2). The deletions were verified by DNA sequencing.

*Hst3Δ97* was created by replacing the 291 3′ base pairs of the *HST3* ORF (which encode for the 97 C-terminal amino acids) with the kanMX cassette as described above, using primers Del F Hst3del97 and Del R Hst3del97 (Table S2) for amplification. The deletion was verified by DNA sequencing.

An additional *sml1Δ* was created using CRISPR/Cas9 manipulations as described below and used as a background strain for generation of *rtt109Δmec1Δsml1Δ* and *rtt109Δrad53Δsml1Δ*. *RTT109* was replaced with the KanMx cassette (*rtt109*::KanMX) using primers from the Yeast Deletion Project (see above), and *MEC1/RAD53* were replaced with the hygromycin B cassette (*mec1/rad53*::hphMX6) amplified from plasmid pAG32 using primers Mec1 F2 and Mec1 R2 for *rtt109Δmec1Δsml1Δ* and primers Rad53 F2 and Rad53 R2 for *rtt109Δrad53Δsml1Δ* (Table S2). The deletions were verified by DNA sequencing.

## METHOD DETAILS

### CRISPR/Cas9 Genetic Manipulations

*swi6Δ*, H3K56Q, H3K56A and H3K56R strains, as well as the additional *sml1Δ* strain, were created using CRISPR/Cas9 manipulations as described in DiCarlo et al., 2013. Briefly, a guide RNA (gRNA) plasmid was created based on pMEL13 (Mans et al., 2015) using RF cloning (van den Ent and Löwe, 2006): the guide RNA cassette was amplified by PCR and used as a mega primer for amplification of the pMEL13 vector. The PCR product was treated with DpnI and transformed into competent bacteria. Colonies were screened using PCR and plasmids were purified by Hi-Yield Plasmid mini kit (RBC Bioscience) from positive clones.

The pMEL13 gRNA was transformed as described above together with p416 (DiCarlo et al., 2013), a Cas9-expressing plasmid, and a repair fragment designed to introduce the desired deletion/point mutation. The deletion/point mutations were verified by DNA sequencing. Primers used for gRNA and oligos used as repair fragments are listed in Table S2. For *swi6Δ*, guide RF primer swi6 F and guide RF primer swi6 R were used for gRNA; SWI6_repair oligo fw and SWI6_repair oligo rv were used as repair fragments. For H3K56Q/A/R, both *HHT1* and *HHT2*, the two genes encoding histone H3, were mutated. K56 guide F and K56 guide R were used for gRNA for mutations of both genes in all three mutants. For *HHT1*, the repair fragments K56Q repair hht1, K56A repair hht1 and K56R repair hht1 were used for H3K56Q, H3K56A and H3K56R, respectively. For *HHT2*, the repair fragments K56Q repair hht2, K56A repair hht2 and K56R repair hht2 were used for H3K56Q, H3K56A and H3K56R, respectively. Mutations were verified by DNA sequencing. For *sml1Δ* used as a background for creating *rtt109Δmec1Δsml1Δ* and *rtt109Δrad53Δsml1Δ*, guide RF primer sml1 F and guide RF primer sml1 R were used for gRNA; SML1 repair oligo fw and SML1 repair oligo rv were used as repair fragments.

### Cell-cycle synchronization and release to HU or YPD

Prior to synchronization cells were grown in YPD for 36 hours at 30°C. The cells were then inoculated in fresh YPD and grown overnight, calculated to reach $OD_{600}$ of 0.12-0.2. Cells were then centrifuged (4000 rpm, 1 min) to remove secreted Bar1 from the media. Following centrifugation, cells were resuspended in pre-warmed YPD containing 5 μg/ml α-factor and incubated at 30°C for 3 hours. After 2.5 hours of synchronization, cells were checked for the presence of shmoos using a microscope.

Release from synchronization was done by washing the cells once with pre-warmed YPD (4000 rpm, 1 min). Following the wash the YPD was discarded and cells were resuspended in pre-warmed YPD or pre warmed YPD containing 200 mM HU and grown for 3-5.5 hours.

Samples were taken for RNA sequencing, DNA sequencing and DNA staining (data not shown) at different time points. At each time point, 3*1.5 mL of the culture was centrifuged (1 Eppendorf per application, 13000 rpm, 12′′) and the supernatant was discarded. Samples for RNA and DNA sequencing were flash frozen in liquid nitrogen, and samples for DNA staining were resuspended in 0.5 mL ice-cold 70% EtOH.

For each mutant in the screen and experiments done in the screen format, 4 time points were taken: 3 hours into α-factor synchronization, and 30, 90 and 180 min following release into HU. For the longer time courses of WT, *rtt109Δ*, *mec1Δsml1Δ*, *rad53Δsml1Δ*, and *Hst3Δ97*, samples were taken every 6min in the first hour and subsequently every 10 minutes for up to 4 hours. For the longer time courses of *paf1Δ* and *ctr9Δ*, time-points were taken every 10 minutes for 5.5 hours. For *rtf1Δ*, *set1Δ,* and *set1Δpaf1Δ*, time-points were taken every 20 minutes for 240 minutes or 320 minutes for the latter. For *rtt109Δ mec1Δsml1Δ & rtt109Δ rad53Δsml1Δ* time points were taken every 20 minutes for 4 hours.

For strains synchronized and released to YPD, with the exception of *rtf1Δ* and *set1Δ*, time-points were taken every 3 minutes for the initial 39 minutes and subsequently every 6 minutes up to 135 minutes. For *rtf1Δ* and *set1Δ*, time points were taken every 6 minutes for the initial 60 minutes and subsequently taken every 10 minutes up to 140 minutes.

### DNA extraction and library preparation

In order to break the cell wall, flash-frozen cells were resuspended in 200 μl lyticase buffer (1M sorbitol, 100 mM EDTA pH = 8.0, 5U/ml lyticase), transferred to a 96-well plate and incubated at 30°C for 30 min. Following incubation, the plate was centrifuged (3000 rpm, 10 min) and the supernatant was discarded. Spheroblasts were resuspended in 100 μl lysis buffer (50 mM HEPES-KOH pH = 7.5, 140 mM NaCl, 1mM EDTA, 1% Triton X-100, 0.1% sodium deoxycholate). 2 μl RNase (5 mg/ml) were added to each well and samples were incubated at 37°C for 60 min. 10 μl Proteinase K (20 mg/ml) and 1 μl glycogen were added to each well and samples were further incubated at 37°C for 2 hours. Samples were then sonicated using a Diagenode Bioruptor Plus (20 cycles, high intensity, 30'' on, 30'' off). 40-60 μl of the sonicate were used to prepare a multiplexed library for sequencing as described in Blecher-Gonen et al., 2013. Libraries were sequenced in an Illumina HiSeq 2500 or Illumina NextSeq 500 with 50 base-pair reads.

### RNA extraction

RNA extraction was performed using a modified protocol of the Nucleospin 96 RNA kit (Machrey-Nagel, 740709). Cell lysis was done in a 96 deep-well plate by adding 450 μL of lysis buffer containing 1 M sorbitol (Sigma-Aldrich), 100 mM EDTA, and 0.45 μL lyticase (10 IU/μL). The plate was incubated in 30°C for 30 min to break the cell wall and then centrifuged for 10 min at 3000 rpm, and the supernatant was removed. From this stage, extraction proceeded as in the protocol of the Nucleospin 96 RNA kit, substituting β-mercaptoethanol with DTT.

### RNA sequencing

For all samples sequenced by Illumina HiSeq 2500, RNA libraries were created as follows: fragmented, poly(A)-selected RNA extracts of ~200 bp size were reverse-transcribed to cDNA using barcoded poly(T) primers. cDNA was amplified and sequenced with Illumina HiSeq 2500 using a primer complementary to the opposite adaptor to the poly(A).

For all samples sequenced by Illumina NextSeq 500, RNA libraries were created as follows: poly(A) RNA was selected for by reverse transcription with a barcoded poly(T) primer. The barcoded DNA-RNA hybrids were pooled and fragmented by a hyperactive variant of the Tn5 transposase (courtesy of Ido Amit). Tn5 was stripped off the DNA by treatment with SDS 0.2% followed by SPRI cleanup and the cDNA was amplified and sequenced with Illumina NextSeq 500.

### ChIP-seq

ChIP-seq was performed using cells synchronized with α-factor for 3 hours and then released into HU for 3-5 hours as described above. Following the 3 hours of α-factor synchronization and 1, 2, 3, and 5 hours of HU treatment, 50 mL of culture were harvested for ChIP for each antibody used. WT and *rtt109Δ* cells were also harvested following 3 hours of HU treatment with no prior synchronization (Figure 5A, asterisk-marked strains). Cells were crosslinked with 1% formaldehyde for 5 minutes at 30°C. The crosslinking was stopped by adding glycine to a final concentration of 125mM and incubating at room temperature for 5 min. Cells were then washed twice with ice-cold DDW (3800 rpm, 4°C, 2-5 min) and flash frozen. ChIP was performed using Dynabeads Protein G (Invitrogen) that were incubated overnight with the appropriate antibody. Cells were resuspended in lysis buffer (50mM HEPES-KOH pH = 7.5, 140mM NaCl, 1mM EDTA, 1% Triton X-100, 0.1% sodium deoxycholate with freshly added Protease Inhibitor Cocktail IV (Calbiochem)) and lysed mechanically with zirconium oxide beads in a BBX24-Bullet Blender (Next Advance). Lysates were then sonicated using a Diagenode Bioruptor Plus (35 cycles, high intensity, 30'' on, 30'' off). The sonicates were pre-cleared by incubation with Dynabeads Protein G incubated in binding/blocking buffer (PBSx1, 0.5% Tween, 0.5% BSA) for 1 hour at 4°C and subsequently incubated with antibody-coupled beads overnight. ChIP libraries were prepared as described in Blecher-Gonen et al., 2013 and sequenced using Illumina NextSeq 500.

### Whole Cell Extracts and Immunoblotting

Whole cell extracts were prepared from 5ml cell extracts ($OD_{600nm}$ = 0.2-0.4) that were flash frozen using liquid nitrogen using standard NaOH extraction: cells were incubated in NaOH 0.1M for 5 minutes. The samples were then centrifuged (3000 rpm, 3 minutes) and the supernatant was discarded. Samples were resuspended in SDS sample buffer (60 mM Tris-HCl pH = 6., 5% glycerol, 2% SDS, 0.025% bromophenol blue, 0.1M DTT) and boiled at 95°C for 5 minutes, and then centrifuged for 10 minutes at 4000 rpm. The supernatant was transferred to a clean tube and 5 μl of each sample were diluted in SDS sample buffer for measuring protein concentration.

Protein concentrations were measured using the Pierce 660nm Protein Assay (Thermo Fisher Scientific) with the Ionic Detergent Compatibility Reagent (IDCR), as described in the protein assay instructions, using the microplate procedure. 4 μg samples were then prepared and resolved by SDS-PAGE.

Proteins were transferred to a nitrocellulose membrane in a submerged tank. Following blocking of the membrane with TBS-T+5% BSA, membranes were blotted with primary antibodies anti-H3K56ac (1:2500, Active Motif) and anti-Actin (1:5000, MP Biomedicals)

and secondary antibodies anti-rabbit HRP (1:15000, Cell Signaling Technology) and anti-mouse HRP (1:10000, Cell Signaling Technology), respectively. Enhanced chemiluminescence was performed using EZ-ECL (Biological Industries).

## QUANTIFICATION AND STATISTICAL ANALYSES

### Processing and analysis of RNA-seq data

Regardless of library preparation method (see above), reads from each RNA-seq sample were mapped to the *S. cerevisiae* genome (SGD, R64-1-1) using Bowtie (parameters:–best –a –m 2 –strata −5 10) (Langmead et al., 2009). Reads mapped to rRNA were disregarded. For the tighter time-courses in Figures 1E, 4C, and 6C the aligned filtered reads were down sampled to 400,000 reads and normalized using unique molecular identifiers (Kivioja et al., 2011). Expression of each gene was quantified as the sum of all reads aligned to the region between 400bp upstream of the 3′ end and 200bp downstream of it. Genes with high sequence similarity in the summed region, in which sequence alignment was similar, were quantified according to the amount of uniquely mapped sequences (Voichek et al., 2016). Total expression was normalized to have a sum of 10^6, and log2 transformed. Genes with normalized expression > log2(10) were taken for further analysis.

### Processing and analysis of ChIP-seq and genomic DNA data

Initial processing of ChIP-seq and genomic DNA sequencing was carried out as follows: genomic tracks were created from the sequence reads, representing the enrichment on each position of the genome. Physical fragment length was estimated by the shift best aligning the mapped sequenced reads from both ± strands, and single-end sequence reads were then lengthened accordingly (in the range of 175-250bp). The signal from each sample was then normalized to obtain the same total signal ($10^8$). For further analysis the average signal was calculated on either gene coding regions or 5Kb genomic bins, and 10Kb specifically for *rtt109Δmec1Δsml1Δ* and *rtt109Δrad53Δsml1Δ*. The average of each genomic bin was calculated on disjoint bins covering the full genome. Averages of genes/bins were then log2 transformed.

#### *Normalizing signal using linear fit*

To normalize data Y by data X using a linear fit, the linear fit (Y = aX+b) between them was calculated, and Y was normalized by subtracting aX+b.

#### *Visualization of DNA replication on a full chromosome (e.g Figure 1C)*

Each 5Kb genomic bin was normalized to its α-factor time point, using a linear fit. For visualization purposes we estimated the total amount of DNA along the time-courses, as previously described (Bar-Ziv et al., 2016). Shortly, DNA sequencing is invariant to total amount of DNA in the cells, thus when comparing two samples, one can only detect a relative change between two regions. The total DNA content was estimated along the time-course of entry into HU. The decrease in DNA content in a specific region accounts for an increase in a different region of the genome. Thus, the data was normalized such that the average of co-replicating regions is monotonically increasing.

#### *Plot of average expression and fit calculation*

For every gene $g$, and every time point $t_i$ following release from α-factor synchronization into HU, the log2 expression of the synchronized time point was subtracted from the log2 expression of time point $t_i$: $\Delta Exp_g^{t_i} = \log_2(Exp_g^{t_i}) - \log_2(Exp_g^{\alpha-factor})$. For each relevant group of genes (e.g., G1 genes), the average $\Delta Exp_g^{t_i}$ was calculated for all time points. To calculate the fit, every 4 adjacent time-points were averaged and the fit was calculated on theses averages. Note: In the *Δrad53Δsml1* time-course (Figure S5A) the 36 minute time point wasn't used in the fitting, as it seems to have some specific noise.

#### *Grouping genes by their replication pattern*

For all tight time-courses (WT, *rtt109Δ*, Figure 1E; *mec1Δsml1Δ*, *rad53Δsml1Δ,* Figure 6C; *paf1Δ*, *ctr9Δ,* Figure 4C; *rtt109Δ set1Δ,* Figure S3I; *Hst3Δ97*, Figure S5M; *rtt109Δmec1Δsml1Δ*, *rtt109Δrad53Δsml1Δ,* Figure S5N) we used the binned DNA data to define regions replicated with the same dynamics upon HU treatment. For each strain, every time-point in HU was normalized by the α-factor time-point. For *paf1Δ* and *ctr9Δ,* only time-points following 1h or more of HU treatment were used, as replication began only after ~2h of HU treatment. For these strains, the average over all time points between α-factor synchronization and 30 min of HU treatment was used for normalization. The genomics bins were then clustered according to their pattern of change over time, using k-means (*kmeans* MATLAB function). This procedure was repeated 275 times, 25 times for each cluster size from size $k = 5$ to size $k = 15$. Following clustering, each gene was assigned to the genomic bin that covers most of its coding region, and thus every clustering defines a grouping both of the genome and a corresponding grouping of the genes.

We also create an *'Mrc1 specific'* grouping by clustering the DNA according to the combination of all the following short time courses: $mrc1^{AQ}$, *mrc1-C14*, Mrc1-MYC, *mrc1Δ*, *ctf18Δ,* and *ctf8Δ*.

#### *Metagene analysis (e.g., Figure 3C)*

Metagene analysis was quantified as follows: the signal of each relevant gene was taken 400bp upstream its transcription start site (TSS) to 400bp downstream of its transcription termination site (TTS) (Pelechano et al., 2013). The region between TSS+200bp to TTS-200bp was binned to 20 bins of equal size. Binned region was extended to the same length for all genes for visualization purposes.

### Estimation of origin firing (Figure 2A)

For every experiment in our screen, and every time point (α-factor, 30 min, 90 min, 180 min), the DNA content over 5Kb spanning the center of every confirmed ARS from OriDB database was averaged (Nieduszynski et al., 2007). For every time point following HU treatment this average was divided by the G1 synchronization time point and log2 transformed to obtain an estimate for the firing of this origin of replication.

### Estimation of replication fork velocity (Figure 2A, middle panel)

Replication fork velocity was estimated for all experiments in the screen. For each experiment the regions replicated in the 30 min, 90 min and 180 min time-point were identified from the DNA sequencing data. The DNA sequencing data was binned to 2.5Kb disjoint bins, averaging the coverage in each bin. Each time point following HU treatment in each experiment was normalized to G1 synchronization using linear fit (see above). Regions replicated in the WT strain were identified manually across the genome for all 3 time points. A Hidden Markov Model (HMM) was trained separately for each time point of the manually defined WT replicated regions using the MATLAB '*hmmestimate'* function. The WT learned parameters were then re-adjusted for each experiment using the MATLAB '*hmmtrain'* function. The replicated regions in this dataset were learned by the *'hmmviterbi'* function. Finally, only regions in the genome that expanded over our 3 time points were used for velocity calculations, and only velocities that were calculated on at least 10 different regions were reported.

### Estimating expression homeostasis in synchronized cells released to unperturbed S phase

Estimating the level of expression homeostasis in cells released from G1 synchronization to YPD (e.g., Figure 6A), was done as in Voichek et al., 2016. The 500 earliest- and 500 latest-replicated genes (Yabuki et al., 2002) were used, excluding genes which are cell-cycle- or stress-regulated. For each gene, average expression change relative to G1 synchronization was calculated and log2 transformed. The normalized expression was averaged separately over early and late genes, and the average of late genes was then subtracted from that of the early ones. To obtain the percent increase in early replicated expression, 2 to the power of this difference was multiplied by 100.

### Estimation of expression from replicated regions

To estimate the level of expression buffering $\boldsymbol{h}$, we used gene expression and DNA sequencing. $\boldsymbol{h}$ will quantify how much expression we have from replication versus non-replicated DNA (Where $h=0\rightarrow$ full buffering and $h=1\rightarrow$ no buffering). We quantify it as follows:

For a gene $\boldsymbol{g_r}$, that is replicated in HU:

$$(1+h)E^{\alpha}_{g_r}T^{\alpha}=E^{HU}_{g_r}T^{HU}$$

Where we define: $\boldsymbol{E^{\alpha}_{g_r}}, \boldsymbol{E^{HU}_{g_r}}$ to be the expression of $g_r$ in α-factor or HU relative to all other mRNA, and $\boldsymbol{T^{\alpha}}, \boldsymbol{T^{HU}}$ to be the total amount of mRNA in α-factor or HU, respectively.

For a gene $\boldsymbol{g}_0$ that is not replicated: $\boldsymbol{E^{\alpha}_{g_0}T^{\alpha}=E^{HU}_{g_0}T^{HU}}$, thus:

$$\frac{E^{HU}_{g_r}}{E^{\alpha}_{g_r}}=\frac{\frac{(1+h)E^{\alpha}_{g_r}T^{\alpha}}{T^{HU}}}{E^{\alpha}_{g_r}}=(1+h)\frac{T^{\alpha}}{T^{HU}}\rightarrow \Delta\Delta \mathrm{E_r}=\frac{\frac{E^{HU}_{g_r}}{E^{\alpha}_{g_r}}}{\frac{E^{HU}_{g_0}}{E^{\alpha}_{g_0}}}=\frac{(1+h)\frac{T^{\alpha}}{T^{HU}}}{\frac{T^{\alpha}}{T^{HU}}}=1+\boldsymbol{h}$$

For genes that are replicated only in a fraction $(\boldsymbol{f})$ of the population:

$$E^{HU}_{g_r}T^{HU}=E^{\alpha}_{g_r}T^{\alpha}(f(1+h)+(1-f)1)\rightarrow \frac{E^{HU}_{g_r}}{E^{\alpha}_{g_r}}=\frac{T^{\alpha}}{T^{HU}}(fh+1)\rightarrow \Delta\Delta \mathrm{E_r}=\frac{\frac{E^{HU}_{g_r}}{E^{\alpha}_{g_r}}}{\frac{E^{HU}_{g_0}}{E^{\alpha}_{g_0}}}=fh+1$$

For measurement of relative DNA content using sequencing of genomic DNA:

$$\Delta\Delta \mathrm{D_r}=\frac{\frac{D^{HU}_{g_r}}{D^{\alpha}_{g_r}}}{\frac{D^{HU}_{g_0}}{D^{\alpha}_{g_0}}}=\frac{\frac{DT^{HU}(2f+(1-f)1)}{DT^{\alpha}}}{\frac{DT^{HU}}{DT^{\alpha}}}=f+1$$

Where we define $\boldsymbol{D^t_g}$ to be the DNA content of this gene relative to all other genes at time $\boldsymbol{t}$. $\boldsymbol{DT^t}$ will be the total DNA content at time $\boldsymbol{t}$.

We get that:

$$\Delta\Delta \mathrm{E_r}=\Delta\Delta \mathrm{D_r}h+(1-h)\rightarrow \log(\Delta\Delta \mathrm{E_r})=\log(\Delta\Delta \mathrm{D_r}h+(1-h))\approx \Delta\Delta \mathrm{D_0},h-h=h(\Delta\Delta \mathrm{D_r}-1)\approx hlog(\Delta\Delta \mathrm{D_r})\rightarrow \log(\boldsymbol{\Delta\Delta E_r})\approx \boldsymbol{hlog}(\boldsymbol{\Delta\Delta D_r})$$

* Simulating the latter approximation gives a deviation of ~10%.

### *Estimating the level of expression buffering* ($\boldsymbol{h}$)

To estimate $h$, the genome was grouped according to the pattern of replication upon entry to HU (see above), obtaining different genomic regions replicated at similar times. For all genes found within a certain group $\log_2(\boldsymbol{E}_g^{HU}/\boldsymbol{E}_g^{\alpha})$ was averaged, and for all the genomic bins found in the group, $\log_2(\boldsymbol{D}_b^{HU}/\boldsymbol{D}_b^{\alpha})$ was averaged. For every two groups the later replicated one was subtracted from the earlier replicated one, giving $\log_2(\Delta\Delta D)$ & $\log_2(\Delta\Delta E)$. Thus, we get $\binom{n}{2}$ $\log_2(\Delta\Delta D)$ and $\log_2(\Delta\Delta E)$ values, where $n$ is the number of groups. We then calculated the linear fit between $\log_2(\Delta\Delta D)$ and $log_2(\Delta\Delta E)$, assuming noise in both axes. The fit was calculated $n-1$ times, leaving one group out each time, and taking the median slope as the estimator for $h$. We followed this procedure for all the different groupings we defined, and each time-point was calculated individually.

Thresholds for how to combine information from different groupings was done as following:

1. For tight time courses (Figures 1E, 6C, S3I, and S5M, and *paf1*Δ & *ctr9*Δ in Figure 4C): Grouping was done according to the DNA from the same experiment (275 groupings). Fits are used if at least one ΔΔD satisfy: $\log_2(\Delta\Delta D) > \log_2(1.4)$. An estimate for $\boldsymbol{h}$ is given if at least 50 fits pass the threshold, and a standard deviation between them is $< 0.25$. For the initial time-points of the time courses following HU addition, fits could not be quantified due to no/low replicated regions, in these cases 0 is plotted.
2. For screen results (Figure 2B) & INO80C subunits (Figure S5G): The DNA groupings of WT & *rtt109*Δ tight time-courses (550 groupings) were used. Fits are used if the level of noise is smaller than 0.4. Noise is defined by the average distance of points from the linear fit, divided by the standard deviation of $log_2(\Delta\Delta E)$. An estimate for $\boldsymbol{h}$ is given if at least 50 fits pass the threshold.
3. For semi-tight time-courses (*set1*Δ in Figure 4C and *paf1*Δ*set1*Δ in Figure 4F & *rtf1*Δ in Figure S3F): The DNA groupings of WT & *rtt109*Δ tight time-courses (550 groupings) were used. Fits are used if the level of noise is smaller than 0.35 and at least one ΔΔD satisfy: $\log_2(\Delta\Delta D) > \log_2(1.4)$. An estimate for $\boldsymbol{h}$ is given if at least 50 fits pass the threshold.
4. For follow-up in screen setup (Figures 4E and S5G): For *rad53Δsml1Δ* repeat (Figure S5G), *rad53Δsml1Δ* grouping was used, for *mec1Δsml1Δ* repeat and *mec1-100* and *mec1-101*, *mec1Δsml1Δ* grouping was used (Figure S5G). For MRC1-MYC, *mrc1-C14* & $mrc1^{AQ}$ the *'Mrc1 grouping'* was used (Figure S5G). For PAF1C components, grouping from *paf1Δ* tight time course was used. Fits were used if at least one ΔΔD satisfied $\log_2(\Delta\Delta D) > \log_2(1.3)$, and an estimate for $\boldsymbol{h}$ is given if at least 50 fits pass the threshold, and have a standard deviation of $< 0.25$.
5. For *rtt109Δmec1Δsml1Δ* and *rtt109Δrad53Δsml1Δ* (Figure S5N): Grouping was done according to DNA from the same experiment, using 10Kb bins. Fits were used if the level of noise was lower than 0.35 and at least one ΔΔD satisfied $\log_2(\Delta\Delta D) > \log_2(1.3)$. An estimate for $\boldsymbol{h}$ is given if at least 25 fits pass the threshold, and have a standard deviation of $< 0.25$.

- In all cases where standard deviation is presented, it was calculated over the fits used to quantify the level of expression buffering $\boldsymbol{h}$.

### Estimation of Pol II, H3K4me2 or H3K4me3 on replicated regions

Estimates of Pol II, H3K4me2 or H3K4me3 on replicated regions were calculated as the expression buffering ($\boldsymbol{h}$), with the following modifications: First, instead of expression level, average ChIP-seq signal over genes was used. The groupings were taken according to the same strain's tight time-course experiment, except for Pol II in *set1Δ, tos4Δ* and *set1Δpaf1Δ,* where grouping was taken from the WT. The fits were then averaged on all 275 groupings, and used as the estimate for the relevant signal on replicated regions.

## DATA AND SOFTWARE AVAILABILITY

RNA-seq, ChIP-seq, and DNA-seq data from this study have been submitted to SRA under BioProject PRJNA438153.